Tectonics

RESEARCH ARTICLE
10.1029/2020TC006553

Key Points:

- 2D numerical models elucidate evolution of asymmetric Kenya Rift segments
- Intrabasinal faulting is caused by bending of the central block and does not reach the brittle-ductile transition
- Small-scale crustal inheritance can exert decisive control on first-order rift architecture

Correspondence to:
S. Brune,
brune@gfz-potsdam.de

Citation:
Richter, M. J. E. A., Brune, S., Riedl, S., Glerum, A., Neuharth, D., & Strecker, M. R. (2021). Controls on asymmetric rift dynamics: Numerical modeling of strain localization and fault evolution in the Kenya Rift. *Tectonics*, *40*, e2020TC006553. https://doi.org/10.1029/2020TC006553

Received 29 SEP 2020
Accepted 7 APR 2021

Controls on Asymmetric Rift Dynamics: Numerical Modeling of Strain Localization and Fault Evolution in the Kenya Rift

Maximilian J. E. A. Richter[1,2], Sascha Brune[1,2], Simon Riedl[2], Anne Glerum[1], Derek Neuharth[1,2], and Manfred R. Strecker[2]

[1]GFZ German Research Centre for Geosciences, Potsdam, Germany, [2]Institute of Geosciences, University of Potsdam, Potsdam, Germany

Abstract Complex, time-dependent, and asymmetric rift geometries are observed throughout the East African Rift System (EARS) and are well documented, for instance, in the Kenya Rift. To unravel asymmetric rifting processes in this region, we conduct 2D geodynamic models. We use the finite element software ASPECT employing visco-plastic rheologies, mesh-refinement, distributed random noise seeding, and a free surface. In contrast to many previous numerical modeling studies that aimed at understanding final rifted margin symmetry, we explicitly focus on initial rifting stages to assess geodynamic controls on strain localization and fault evolution. We thereby link to geological and geophysical observations from the Southern and Central Kenya Rift. Our models suggest a three-stage early rift evolution that dynamically bridges previously inferred fault-configuration phases of the eastern EARS branch: (1) accommodation of initial strain localization by a single border fault and flexure of the hanging-wall crust, (2) faulting in the hanging-wall and increasing upper-crustal faulting in the rift-basin center, and (3) loss of pronounced early stage asymmetry prior to basinward localization of deformation. This evolution may provide a template for understanding early extensional faulting in other branches of the East African Rift and in asymmetric rifts worldwide. By modifying the initial random noise distribution that approximates small-scale tectonic inheritance, we show that a spectrum of first-order fault configurations with variable symmetry can be produced in models with an otherwise identical setup. This approach sheds new light on along-strike rift variability controls in active asymmetric rifts and proximal rifted margins.

1. Introduction

Asymmetric rifting, which is characterized by a dominant single border fault, is known to have played a major role in the evolution of many past rift systems (e.g., Schlische et al., 2003; Withjack et al., 2013). It can also be observed in many presently active extensional tectonic settings (e.g., Gawthorpe & Leeder, 2008; Ebinger & Scholz, 2011), where it governs basin geometry, topography evolution, erosion, and sedimentation patterns. One such setting is the largest continental rift system in existence today: the East African Rift System (EARS). It exhibits a wide array of developmental stages from youthful extension with incipient faulting to final continental breakup (Corti, 2009; Ebinger & Scholz, 2011; Ring, 2014) and is thus an ideal location for studying the stages of early rifting that involve asymmetric normal fault activity followed by hanging-wall segmentation. In this study, we focus on the southern and central sectors of the Kenya Rift, which are in an early phase of active continental rifting (Ebinger et al., 2017) characterized by the transition from waning border fault activity to enhanced intra-basinal faulting and subsidence (Muirhead et al., 2016).

The first-order tectonic characteristics of continental rifts are known to be influenced by a large range of structural, petrological, and thermal parameters, which have been investigated in previous numerical modeling studies (e.g., Armitage et al., 2018; Duretz et al., 2016; Huismans & Beaumont, 2011; Jammes & Lavier, 2019; Naliboff et al., 2017; Petersen & Schiffer, 2016). It is evident that, in addition to the rheological characteristics of crust and mantle (thickness, composition, and intrinsic heterogeneity), the thermal structure, which includes the effects of radiogenic heating, plays a major role in rift evolution (e.g., Burov & Schubert, 2007). Depending on these parameters, either wide or narrow (e.g., Brun, 1999; Buck et al., 1999) and either symmetric or asymmetric rifts (Buiter et al., 2008; Huismans and Beaumont, 2003) may form. Although the above processes dictate the principal rift setting, the location, orientation, and geometry of

the initial fault systems may be strongly affected by pre-existing structures and fabrics associated with suture zones (e.g., Corti, 2009; Corti et al., 2007; Delvaux et al., 2012; Hodge et al., 2018; Phillips et al., 2016; Shackleton, 1993; Smith & Mosley, 1993).

The structural evolution of continental rifts is controlled to a large degree by the influence of tectonic and magmatic processes (e.g., Buck et al., 2005) whose impact can be sketched by considering two end-members: (1) In magma-assisted rifts, such as in the Afar region (Kendall et al., 2005), dikes and other magmatic intrusions accommodate the majority of overall extensional deformation (Bastow & Keir, 2011) and play a vital role in achieving continental breakup (Wright et al., 2006). (2) Conversely, in tectonically dominated rifts, deformation is accommodated by faults while only a minor part of the extensional deformation is related to magmatic processes (e.g., Petit & Deverchere, 2006; Schumacher, 2002; Schwarz & Henk, 2005). The eastern branch of the EARS, however, does not clearly belong to one of these end-member cases as upper crustal extension is accommodated by a combination of normal faulting and diking (Calais et al., 2008; Muirhead et al., 2015; Oliva et al., 2019). Voluminous lava flows that testify to widespread thermal processes and volcanic activity are documented throughout the history of the eastern branch (Rooney, 2020). Nevertheless, the details of how magmatic contributions influence the development of first-order tectonic structures in this area are not well understood.

Many numerical modeling studies have focused on continental margins (e.g., Bassi, 1991; Brune et al., 2014; Huismans & Beaumont, 2011; Salazar-Mora et al., 2018; Svartman Dias et al., 2015; Tetreault & Buiter, 2018), while analogue modeling techniques have largely been used to study the structural evolution of active continental rifts and their geodynamic causes (e.g., Corti, 2012; Khalil et al., 2020; Sokoutis et al., 2007; Zwaan et al., 2019). The reason why analogue techniques are often preferred in these settings is the comparably high spatial resolution that allows the details of the evolution of normal-fault networks to be captured, especially during early rifting where crustal thinning is limited. In contrast, the advantage of numerical models lies in their ability to reproduce the temperature- and strain-rate-dependent rheological evolution of the lithosphere, which is particularly important during the necking and crustal hyper-extension phases that have shaped many rifted margins worldwide (Jeanniot & Buiter, 2018; Péron-Pinvidic et al., 2019). Hence, only a small number of numerical geodynamic modeling studies have focused on active continental rifts (e.g., Beutel et al., 2010; Corti et al., 2019; Muluneh et al., 2020), and many of those studies have addressed either large-scale processes of rifting and the driving forces responsible (Kendall & Lithgow-Bertelloni, 2016; Stamps et al., 2015; Ulvrova et al., 2019) or the interaction between volcanism and mantle dynamics (Armitage et al., 2018; Civiero et al., 2019; Koptev et al., 2018). Nevertheless, significant insights into the early stages of the structural evolution of rifts may be gained from studying individual sectors of active rifts and comparing geological information and interpretations of tectonic evolution with numerical models. This holds especially true for the effects of rheology, thermal structure, and inheritance on localization patterns, geometry, and timing of faults, and the resulting interaction between magmatic and structural processes.

In this study, we employ numerical 2D forward models to analyze the evolution of early rift stages. We establish a reference model that reproduces major aspects of the Southern and Central Kenya Rifts, where a good coverage of geological and geophysical data is available. Our aim is to understand how and why an asymmetric, narrow rift forms in this particular geological setting and to discuss its tectonic evolution.

2. Geological Background

The Kenya Rift (36°E, 3°N to 2°S), where asymmetric and symmetric rift geometries are observed, exhibits many key aspects of rift evolution (Figure 1). It is a slowly spreading, active continental rift, with a present-day extension rate of ~2 mm a^{-1} (e.g., Saria et al., 2014). The Kenya Rift is part of the eastern branch of the EARS and is located within the nascent plate boundary between the Somalia and Victoria plates (Stamps et al., 2008, Figure 1a). Major east-dipping normal faults on the western side of the rift and normal faults with lesser throws that cut the eastern flanks of the rift led to the formation of a pronounced basin with an average width of 60–70 km (Figure 1b). The interior of this basin, however, became increasingly dissected by arrays of closely spaced, low-offset normal faults that delimit a tectonically active depression (Baker et al., 1988), which constitutes an inner graben.

10.1029/2020TC006553

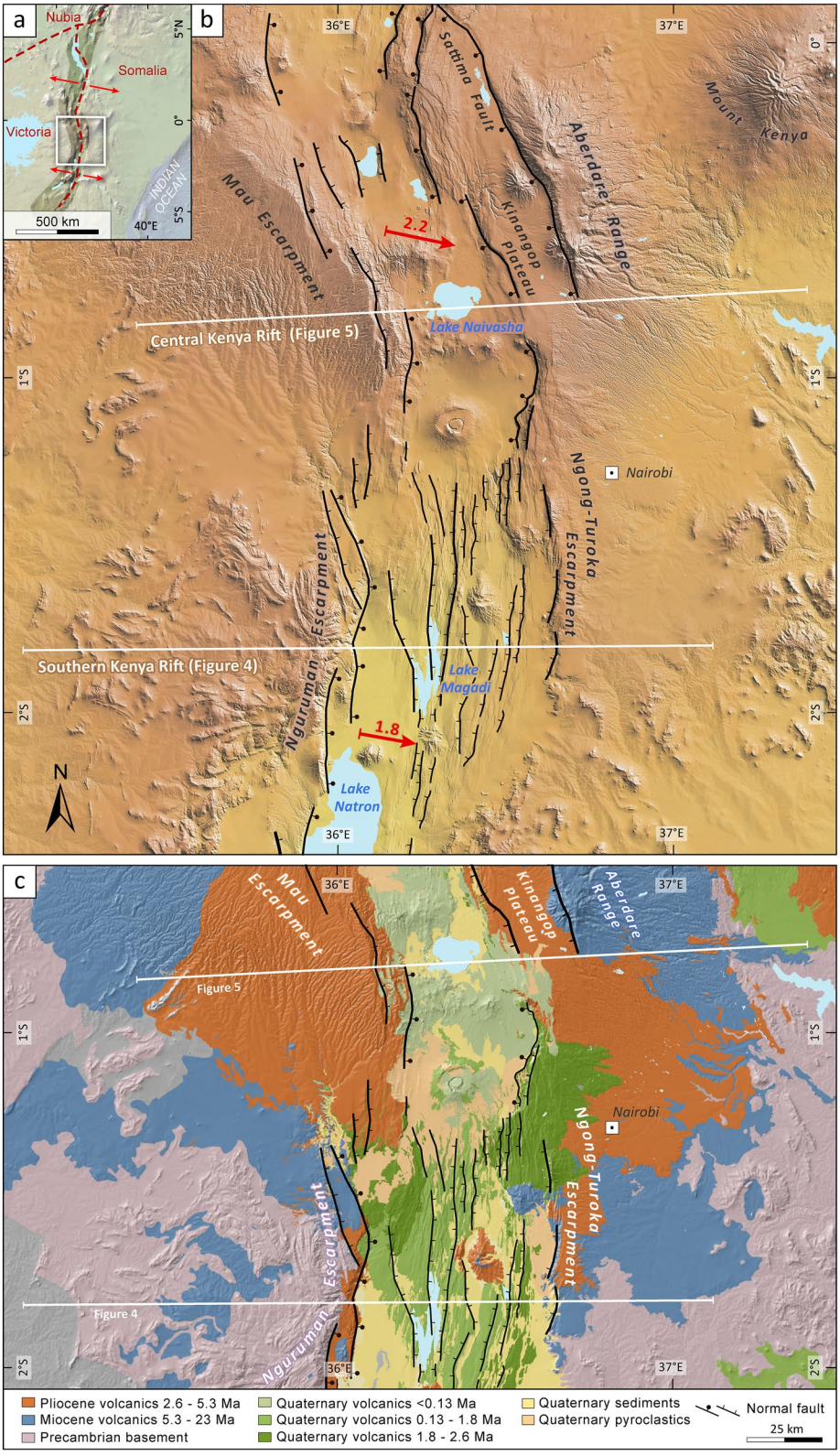

Based on the overall fault geometry, our study region (Figure 1b) can be divided into two sectors. The first consists of the asymmetric north-northeast-oriented Southern Kenya Rift with one major border fault along the Nguruman Escarpment in the west, and a ~50 km wide and densely faulted inner rift sector, which slopes gently toward the west. The eastern side of the Southern Kenya Rift is bordered by the prominent Ngong-Turoka Escarpment, which constitutes an antithetically faulted flank (Baker et al., 1988; Smith, 1994). The second sector consists of the asymmetric northwest-oriented Central Kenya Rift (Figure 1b) with the Mau Escarpment on the west and the antithetic Sattima and Kinangop faults on the east (Baker et al., 1988; Shackleton, 1945). Overall, fewer secondary faults are exposed in this region due to the masking effect of ubiquitous Quaternary pyroclastic deposits.

Across the Nguruman Fault at the western flank of the Southern Kenya Rift, elevation decreases from ~1,800 m at the rift shoulder to ~600 m at the rift floor (e.g., Baker, 1958; Crossley, 1979). The fault has an approximate dip of 60°–65° E at the surface and appears to be shallowing slightly at depth as suggested by local seismicity (Lee et al., 2016; Weinstein et al., 2017). In contrast, the eastern rift flank has a less pronounced relief and exposes westward-dipping Neogene volcanics (Pliocene Trachytes; Baker et al., 1988; Randel & Johnson, 1970) of the Ngong-Turoka Escarpment, with a height of at least 350 m above the downfaulted equivalents of the Pliocene Trachytes within the rift that are exposed at the surface (Baker & Mitchell, 1976). Farther basinward of these outcrops, elevation decreases along densely spaced, rift-parallel horst-and-graben structures, which characterize the entire area from the eastern side of the rift to the basin floor in the Magadi area. The current depocenter and sediment sink of the Southern Kenya Rift is the Magadi–Natron lake basin at ~600 m elevation, situated between the rift center and the western border fault (Figure 1).

2.1. Timing of Rifting

The present-day configuration of the Southern and Central Kenya Rift is associated with extensional processes that began during the Miocene (e.g., Shackleton, 1978; Tiercelin & Lezzar, 2002). However, thermochronological, geophysical, and sedimentary evidence for a preceding rifting episode during the Paleocene–Eocene exists immediately north of the equator in the transition between the Central and the Northern Kenya Rift (e.g., Ego, 1994; Hautot et al., 2000; Mugisha et al., 1997; Torres Acosta et al., 2015).

The onset of Miocene extensional faulting in the Central Kenya Rift was closely linked with the emplacement of extensive phonolite flows (Shackleton, 1945; Baker et al., 1971, 1988; Lippard, 1973) that were deposited in a shallow, wide depression (Lippard, 1973, Figure 1c, blue Miocene units). This depression existed at 14.5 Ma, as it unconformably encloses flood phonolites of that age that overspilled these areas and flowed away from the future rift area (Lippard, 1973; Williams, 1972; Wichura et al., 2010, 2015). These areally extensive flood phonolites are widespread on the shoulders of the Central Kenya Rift (mainly mapped as Middle Miocene Plateau Phonolites), where they serve as important strain markers. The earliest faults cutting these Middle Miocene Plateau Phonolites were active at the western side of the present-day rift in the transition to the Northern Kenya Rift, documenting the onset of down-to-the-east normal faulting and the formation of a half-graben between 14.5 and 12 Ma at ~1° N (Chapman & Brook, 1978; Hetzel & Strecker, 1994; Morley et al., 1992; Mugisha et al., 1997), which is also reflected by thermochronological records showing a rapid cooling phase beginning at that time (Torres Acosta et al., 2015). These fault scarps prevented subsequent lavas flows of the Upper Miocene Flood Phonolites and Trachytes from overflowing the rift toward the west (Baker et al., 1971; Crossley, 1979). In the Central Kenya Rift, this half-graben geometry is associated with the east-dipping normal faults that constitute the Mau Escarpment (Clarke et al., 1990, Figure 1). An asymmetric geometry can be unambiguously documented using the ubiquitous occurrence of the Mio-Pliocene Plateau Trachytes that are exposed at 2,700 m elevation on the eastern (Saggerson, 1970)

Figure 1. (a) Plate-tectonic overview and (b) simplified map of the Southern and Central Kenya Rift with normal faults (black), location of cross sections (white), and present-day full extension velocities (red arrows) in mm a^{-1} (based on Saria et al., 2014). The Southern Kenya Rift extends from ~2.5° to ~1°S and is bounded by the Nguruman Escarpment to the west. The Central Kenya Rift is bounded by the Mau Escarpment and extends from ~1°S to ~2.5°N (not shown on this map). Ball-and-bar symbol denotes important faults with throws >500 m, mainly along the western rift-bounding border faults and the Sattima Fault of the central segment. The local extension direction is nearly rift-perpendicular in the area of the analyzed cross sections, justifying a 2D modeling approach, although evidence for oblique extension exists in the Central Kenya Rift (Zielke & Strecker, 2009). (c) Geological overview of the study area (based on the Geological Map of Kenya, 1987, and Guth, 2014). The geology of the rift shoulders is shown without Quaternary sedimentary and volcanic air-fall covers.

and western (Williams, 1969a) rift shoulders and at ~2,500 m on the fault-bounded intrarift Kinangop Plateau (Figure 1; Baker et al., 1971, 1988) in contrast, this unit has been downfaulted by 1,000 m along the Mau Escarpment with a pronounced westward dip that indicates the dominance of the western border fault during asymmetric rifting (Clarke et al., 1990).

At the present-day eastern side of the Central Kenya Rift, Early Pliocene faulting generated throws between 500 and 700 m along the west-dipping Sattima Fault (Figure 1) testifying the transition to a morphologic full-graben stage (e.g., Shackleton, 1945). This was followed by normal faulting farther west prior to 2.6 Ma that formed the array of faults bounding the Kinagop Plateau to the west and delimiting the ~40-km-wide inner graben (Baker et al., 1988; Clarke et al., 1990). Due to the sustained subsidence along faults that bound the inner graben, the areal extent of volcanic and sedimentary units became increasingly limited with decreasing age. As such, Quaternary volcano-sedimentary units are areally restricted to the inner graben, which has been the focus of densely spaced normal faulting that has resulted in a horst-and-graben landscape (Hackman, 1988; McCall, 1967; Thompson & Dodson, 1963). Furthermore, the inner graben has been characterized by volcanic, seismic, and hydrothermal activity during the last 2 Ma (Clarke et al., 1990; Riedl et al., 2020; Tongue et al., 1992).

The first manifestations of extensional tectonism in the Southern Kenya Rift are documented at <10 Ma (Crossley, 1979) along the western Nguruman Escarpment, whereas the eastern rift border along the Ngong-Turoka Escarpment was faulted only during the Pliocene (Baker & Mitchell, 1976; Saggerson, 1991). Over time, fault activity migrated from the Nguruman Escarpment eastward to the Lake Magadi basin in the center of the rift (Baker, 1958; Crossley, 1979). Here, the youngest volcanic units are the 0.95 to 1.37 million-year-old Magadi Trachytes that are confined to the inner graben (Baker et al., 1971), and stratigraphically equivalent trachyte flows occur throughout the Kenya Rift in similar, fault-bounded structural settings. All of these units are affected by densely spaced normal faults (e.g., Baker et al., 1988; Muirhead et al., 2016) that define the seismically active volcano-tectonic axis of the rift. In the Magadi area young tectonic activity is documented by small-offset normal-faults (e.g., Hillaire-Marcel et al., 1986; Muirhead et al., 2016) and numerous extensional cracks that strike parallel to the Quaternary normal faults. Extensional cracks generated during recent earthquakes at the rift floor (Atmaoui & Hollnack, 2003; Muirhead & Kattenhorn, 2018) and pronounced seismic activity (Ibs-von Seht et al., 2001; Weinstein et al., 2017) in the Magadi area document that extensional processes are active today.

3. Numerical Model Setup

Here, we employ numerical forward models to investigate the early stage evolution of asymmetric continental rifting. In doing so, the finite element software ASPECT (Advanced Solver for Problems in Earth's ConvecTion) (Bangerth et al., 2018, 2019; Heister et al., 2017; Kronbichler et al., 2012) is used to solve the thermomechanically coupled conservation equations of momentum (Equation 1), mass (Equation 2), energy (Equation 3), combined with additional advection equations for each Eulerian compositional field c_i (Equation 4):

$$-\nabla \cdot \left(2\eta\dot{\varepsilon}\right) + \nabla P = \rho \mathbf{g} \tag{1}$$

$$\nabla \cdot \left(\mathbf{v}\right) = 0 \tag{2}$$

$$\begin{aligned} \bar{\rho} c_P \left(\frac{\partial T}{\partial t} + \mathbf{v} \cdot \nabla T\right) - \nabla \cdot \kappa \nabla T &= \bar{\rho} H && \text{radioactive heating} \\ &+ \left(2\eta\dot{\varepsilon}\right) : \dot{\varepsilon} && \text{shear heating} \\ &+ \alpha T \left(\mathbf{v} \cdot \nabla P\right) && \text{adiabatic heating} \end{aligned} \tag{3}$$

$$\frac{\partial c_i}{\partial t} + \mathbf{v} \cdot \nabla c_i = 0 \tag{4}$$

Table 1
Model Parameters

Parameter	Units	Upper crust	Lower crust	Lithospheric mantle	Asthenospheric mantle
Reference temperature	K	293	293	293	293
Reference density	kg m^{-3}	2,700	2,850	3,280	3,300
Adiabatic surface temperature	K	1,623	1,623	1,623	1,623
Thermal expansivity	10^{-5} K^{-1}	2.7	2.7	3.0	3.0
Thermal diffusivity	10^{-7} m^2 s^{-1}	7.7160	7.3099	8.3841	8.3333
Heat capacity	J kg^{-1} K^{-1}	1,200	1,200	1,200	1,200
Radiogenic heat production	μW m^{-3}	0.5	0.1	0	0
Unweakened friction coefficient		0.5	0.5	0.5	0.5
Cohesion	MPa	20	20	20	20
Rheology		*Wet Quartzite*[a]	*Wet Anorthite*[b]	*Dry Olivine*[c]	*Wet Olivine*[c]
Unweakened pre-exponential constant for diffusion creep	Pa^{-1} s^{-1}	5.97×10^{-19}	2.99×10^{-25}	2.25×10^{-9}	1.5×10^{-9}
Grain size	mm	1.0	1.0	1.0	1.0
Grain size exponent		2.0	3.0	0	0
Activation energy for diffusion creep	kJ mol^{-1}	223	159	375	335
Activation volume for diffusion creep	cm^3 mol^{-1}	0	38.0	6.0	4.0
Unweakened pre-exponential constant for dislocation creep	Pa^{-n} s^{-1}	8.57×10^{-28}	7.13×10^{-18}	6.52×10^{-16}	2.12×10^{-15}
Power law exponent for dislocation creep		4.0	3.0	3.5	3.5
Activation energy for dislocation creep	kJ mol^{-1}	223	345	530	480
Activation volume for dislocation creep	cm^3 mol^{-1}	0	38.0	18.0	11.0
Softening laws					
Maximum friction softening[d]		90%	90%	90%	none
Maximum viscous softening[e]		90%	90%	none	none

[a]Rutter and Brodie (2004). [b]Rybacki et al. (2006). [c]Hirth and Kohlstedt (2003). [d]Linear decrease of friction coefficient by 90% between strain values of 0 and 0.5. [e]Linear decrease of effective viscosity by 90% between strain values of 0 and 0.5.

where $\dot{\varepsilon}$ is the deviator of the strain rate tensor $\frac{1}{2}\left(\nabla \mathbf{v} + \left(\nabla \mathbf{v}\right)^T\right)$ with $\mathbf{v}$ the velocity vector. Density is defined as $\rho = \rho_0\left(1 - \alpha\left(T - T_0\right)\right)$ with the thermal expansivity α and the reference temperature T_0, while P is the pressure, $\mathbf{g}$ is the gravity vector, $\bar{\rho}$ is the adiabatic reference density, T is the temperature, κ is the thermal diffusivity, and H is radioactive heating. The visco-plastic effective viscosity η_{eff} is computed from either a composite of diffusion and dislocation creep (Equation 5) or Drucker-Prager plasticity (Equation 6; Glerum et al., 2018) depending on whether viscous stresses stay below the yield stress or not.

$$\eta_{eff}^{diff\,|\,disl} = \frac{1}{2}\left(\frac{1}{A}\right)^{1/n} \dot{\varepsilon}_e^{(1-n)/n} \exp\left(\frac{Q + PV}{nRT}\right) \tag{5}$$

where $n = 1$ for diffusion creep and $n > 1$ for dislocation creep and the effective deviatoric strain rate is defined as $\dot{\varepsilon}_e = \sqrt{\frac{1}{2}\dot{\varepsilon}'_{ij}\dot{\varepsilon}'_{ij}}$. Values for prefactor A, activation energy Q, activation volume V, and gas-constant R are given in Table 1. Plastic effective viscosity is given by:

$$\eta_{eff}^{pl} = \frac{C\cos\left(\phi\right) + P\sin\left(\phi\right)}{2\,\dot{\varepsilon}_e} \tag{6}$$

where C is the cohesion and ϕ the friction angle.

For this study, plastic strain is stored on particles (Gassmöller et al., 2018) to reduce fault width and to avoid numerical diffusion of the strain variable. Parameters are listed in Table 1. Here, we build on previous ASPECT setups that were designed to capture rift dynamics on a wide range of scales (Corti et al., 2019; Glerum et al., 2020; Heckenbach et al., 2021; Muluneh et al., 2020; Neuharth et al., 2021; Sandiford et al., 2021).

Our 2D models comprise a 500 × 200 km box with up to 500 m elemental resolution. The initial, prerift structure consists of a 22-km-thick upper crustal layer with a wet quartzite rheology, a 16-km-thick lower crustal layer of wet anorthite, an 82-km-thick lithospheric mantle of dry olivine and an 80-km-thick section of asthenospheric mantle comprised of wet olivine (see Table 1 and Figure 2a). Hence, the initial Moho depth is 38 km, and lithospheric thickness is 120 km. This particular crustal and mantle geometry is inspired by the gravity and thermal models of Sippel et al. (2017), but chosen such that it reflects estimated prerift thicknesses.

We chose a model setup that represents two well-known aspects of East African rifting in a simplified representation:

(1) Structural inheritance. Continental deformation often localizes within zones of past tectonic activity (e.g., Schumacher, 2002; Schlische et al., 2003; Withjack et al., 2013), as is also observed within the EARS (Corti et al., 2007; Katumwehe et al., 2015; Macgregor, 2015; Shackleton, 1993; Smith & Mosley, 1993). Especially basement foliations and reactivation of pre-existing structures or fault geometries are involved in defining the deformation patterns (e.g., Corti, 2009; Delvaux et al., 2012; Hetzel & Strecker, 1994; Morley, 2010). In numerical models, these are either incorporated as prescribed, local features (Corti et al., 2003; Brune, et al., 2017a; Salazar-Mora et al., 2018) or with some form of random noise (Duclaux et al., 2020; Naliboff et al., 2020) to focus localization of the model. Here, we adopt the latter approach by implementing a zone in the model center of randomized initial strains from 0 to 0.2 (see Figure 2a) using a Gaussian distribution with a width of $2\sigma = 200$ km that is comparable to that of mobile belts (Lenardic et al., 2000; Katumwehe et al., 2015). All differences between the models of this study result from a random seed pattern affecting the distribution of the initial strain within this Gaussian envelope (Figure 2a). Note that the employed random number generator *srand* can yield variable patterns for different library configurations; hence, individual model details are currently not reproducible on other computers, only the overall ensemble behavior. To facilitate localization, we use softening laws for (i) brittle layers (e.g., Brune, 2014; Jourdon et al., 2021; Persaud et al., 2017; Petersen & Schiffer, 2016; Salazar-Mora et al., 2018) and (ii) ductile parts of the crust (e.g., Döhmann et al., 2019; Gerbi et al., 2010; Pérez-Gussinyé et al., 2020) (Table 1). Brittle softening is implemented as a linear decrease of the friction coefficient by up to 90% between accumulated strain values of 0–0.5. It is applied to the upper and lower crust and the lithospheric mantle. Viscous softening on the other hand is implemented as a factor that reduces the effective viscous viscosity by up to 90%, again between accumulated strain values of 0–0.5. It is only applied to the crustal layers.

(2) Changes in thermal regime related to the large-scale impingement of a mantle plume. Evidence for the involvement and timing of a mantle plume in East African extension comes from a wide range of geochemical (Halldórsson et al., 2014; Pik et al., 2006), seismological (Civiero et al., 2015; Green et al., 1991; Mulibo & Nyblade, 2013), paleo-topographical (Wichura et al., 2010, 2015), and modeling studies (Koptev et al., 2018; Moucha & Forte, 2011). We account for the plume-affected lithospheric temperature distribution at the onset of extension through the following scheme: Phase I (*pre-plume*) represents stable, equilibrated conditions using a mantle potential temperature of 1,350°C (Rooney et al., 2012) and the lithospheric structure described above starting from a steady-state conductive continental geotherm and an adiabatic temperature increase in the sublithospheric mantle. A temperature increase of the asthenospheric layer due to the arrival of the East-African mantle plume (Hofmann et al., 1997) is simulated in phase II (*pre-rift*) by increasing the bottom temperature boundary condition by 200°C, a generally inferred excess plume temperature (Bunge, 2005; Schilling, 1991), which is somewhat higher than values calculated for potential mantle temperatures based on volcanic rocks of the area (Rooney et al., 2012). After 20 Ma of small-scale convection in the asthenosphere, phase III (*syn-rift)* starts by imposing extensional velocities at the model boundaries. During this phase, a narrow rift initiates and evolves. Due to the simplified setup, we do not account for

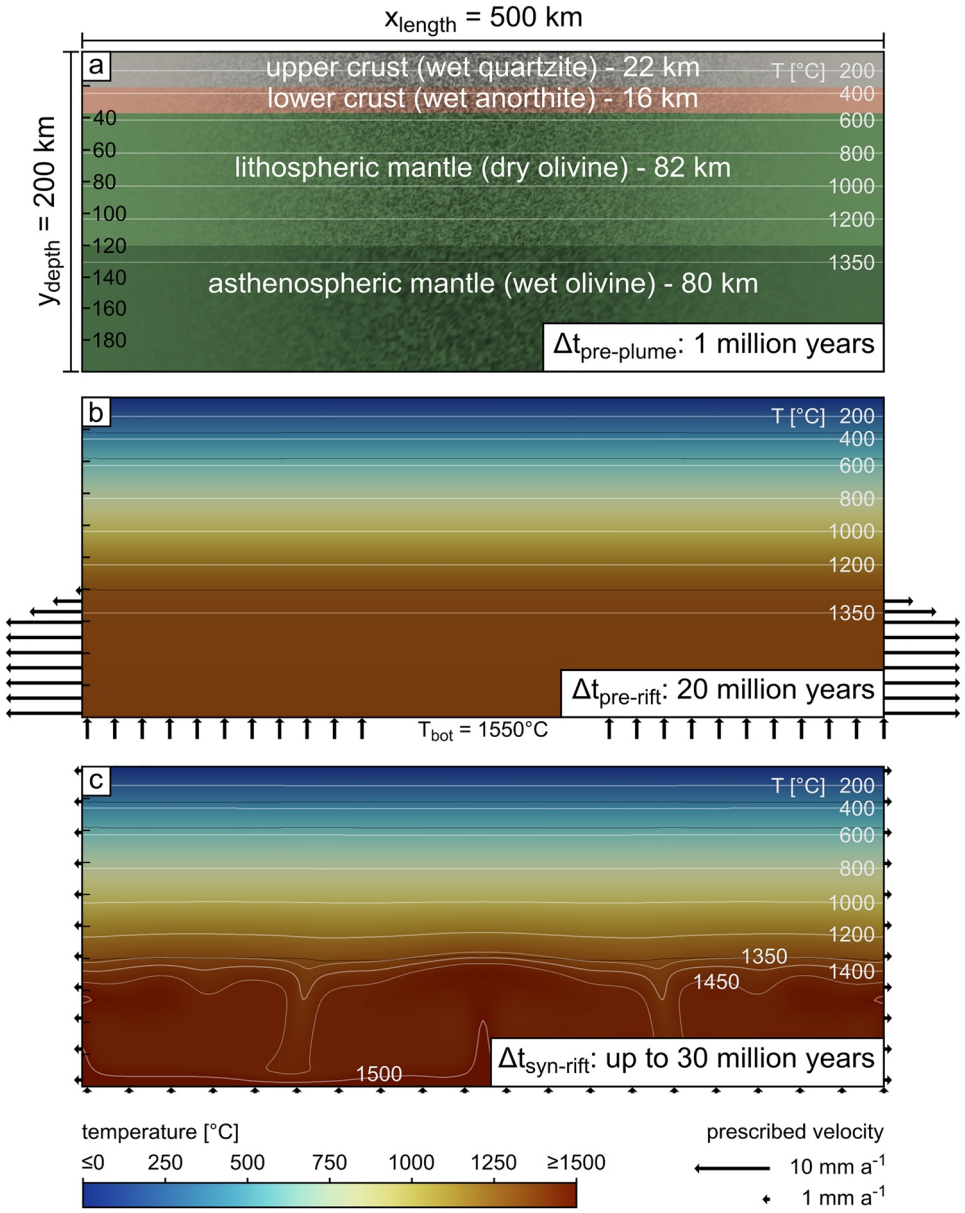

Figure 2. Setup of the numerical model at the start of each of the three model phases. (a) Phase I (pre-plume): Thermally equilibrated setup with prescribed boundary velocities of zero, modeled time: 1 million years. Strain is seeded using a Gaussian distribution of amplitude 0.2 at random locations (dark areas in model center) simulating structural inheritance to facilitate and focus localization. (b) Phase II (pre-rift): Arrival of a hot mantle plume simulated by prescribing an excess temperature of 200°C as bottom boundary condition and a fast divergent asthenospheric flow field. Velocity boundary conditions lead to small-scale convection and a temperature increase in the asthenospheric mantle. (c) Phase III (syn-rift): Start of lithospheric extension with velocity boundary conditions prescribing a full extension velocity of 2 mm a^{-1} (Saria et al., 2014). Note how the mantle temperatures increased due to the previous plume arrival stage, while due to the low conductivity of rocks the shallow temperatures are not affected at all.

other processes that result from plume impingement like diking or lithospheric erosion from below (e.g., Beniest et al., 2017; Celli et al., 2020; Koptev et al., 2015; Sobolev et al., 2011).

The time-dependent velocity and temperature specifications at the model boundaries are complemented by the following thermal and mechanical boundary conditions: a free surface (Rose et al., 2017) with a constant temperature, and thermal isolation at the model sides. Outflux is prescribed on the left and right

boundary and adjusted for each of the model's three phases (see Figure 2); no flow in phase I, strong outflow of up to 10 mm a^{-1} through the left and right sides of the asthenosphere in phase II and 1 mm a^{-1} of outflow through the entire the left and right boundaries in phase III, which reflects estimates of the present-day extension rate in our study region (Saria et al., 2014). In order to conserve model volume, lateral outflow is compensated by prescribed inflow through the bottom boundary.

There are several model limitations that have to be kept in mind when interpreting our results. Our models neither represent magmatic processes like diking and underplating, nor surface processes, dynamic topography, plume-related lithosphere erosion, or 3D effects. Since deeply sourced dynamic topography is excluded from the model, about 1–2 km elevation has to be added when comparing the model results to topography in nature (Faccenna et al., 2019; Moucha & Forte, 2011; Osei Tutu et al., 2018). Another limitation is the uncertainty in radiogenic heat, that has a big impact on deformation patterns and wide or narrow rifting styles (Jaupart et al., 2016), mainly because it affects the thicknesses of the viscous and brittle layers in the upper and lower crust. For the setup of our study we chose the following values for radiogenic heat production: 0.5 μW m^{-3} for the upper crust and 0.1 μW m^{-3} for the lower crust (Jaupart et al., 2016).

4. Modeling Results

4.1. Evolution of the Numerical Reference Models

After the brief pre-plume phase, small-scale convection is observed in the asthenosphere during the pre-rift phase (Figure 2c). The lithosphere-asthenosphere boundary (LAB), which is defined here as the compositional interface between lithospheric and asthenospheric mantle, rose by up to 7 km in the model center due to the small-scale convection. At the end of the pre-rift phase, at a total modeled time of 21 million years, the temperature at the LAB has increased by ~100°C to 1350°C. Interestingly, temperatures in the shallower lithospheric mantle and the crustal layers are barely affected by this temperature increase (Figure 2c), since conductive equilibration in the lithosphere operates over hundreds of millions of years (Cacace & Scheck-Wenderoth, 2016). We also find that significantly longer plume-residence times do not heat the lithosphere enough to induce a shift from narrow to wide rifting. This could only be achieved by more radiogenic heating or higher crustal thicknesses, which indicates that brittle localization has more control on resulting structures than conductive heating from below.

In the first 15 million years of the syn-rift phase, strain does not localize efficiently, and deformation is distributed throughout the entire crustal layer. As faults compete for strain, they successively coalesce until one of the border faults accommodates almost all extension (Figure 3). Meanwhile, the LAB rises by about 10 km and isotherms are advected upwards. At Moho depths, advection transfers heat faster than conduction, even at these slow extension rates. Finally, a narrow rift is established in the model center and the lithospheric layer is thinned further during continued extension. In our reference model for the Southern Kenya Rift, the narrow, asymmetric rift initiates at $t_{10} = 10$ Ma (Figure 3c). Timings are referenced to a state of the numerical model that compares well to the present-day rift (Figure 4). With ongoing deformation, the eastern border fault is established around 5 Ma (Figure 3d). Due to rotation of the major faults in the west, shallow, minor faults develop in the uppermost layer of the hanging-wall in the basin interior. A similar tectonic evolution is observed in our reference model for the Central Kenya rift (Figure 5). The main difference is that the secondary border fault is slightly more active. Hence, the difference in elevation of the rift shoulders is lower.

4.2. Impact of Inheritance

We investigate the impact of small-scale inheritance by introducing element-sized strength perturbation in our models. In nature, these heterogeneities may be represented by foliations, lithological heterogeneities or pore-pressure variations. Here, we approximate this complexity by means of randomly distributed strength variations that are implemented through the combination of frictional strain softening and an initial, random strain distribution. We conduct 26 model runs that are identical to the reference model except for a different random strain pattern at model start. Thereby, we self-consistently generate a range of possible crustal-scale fault configurations, but we also isolate the dominant deformation style of a specific numerical setup by monitoring its frequency across a range of initial noise configurations (Figure 6). Instead of

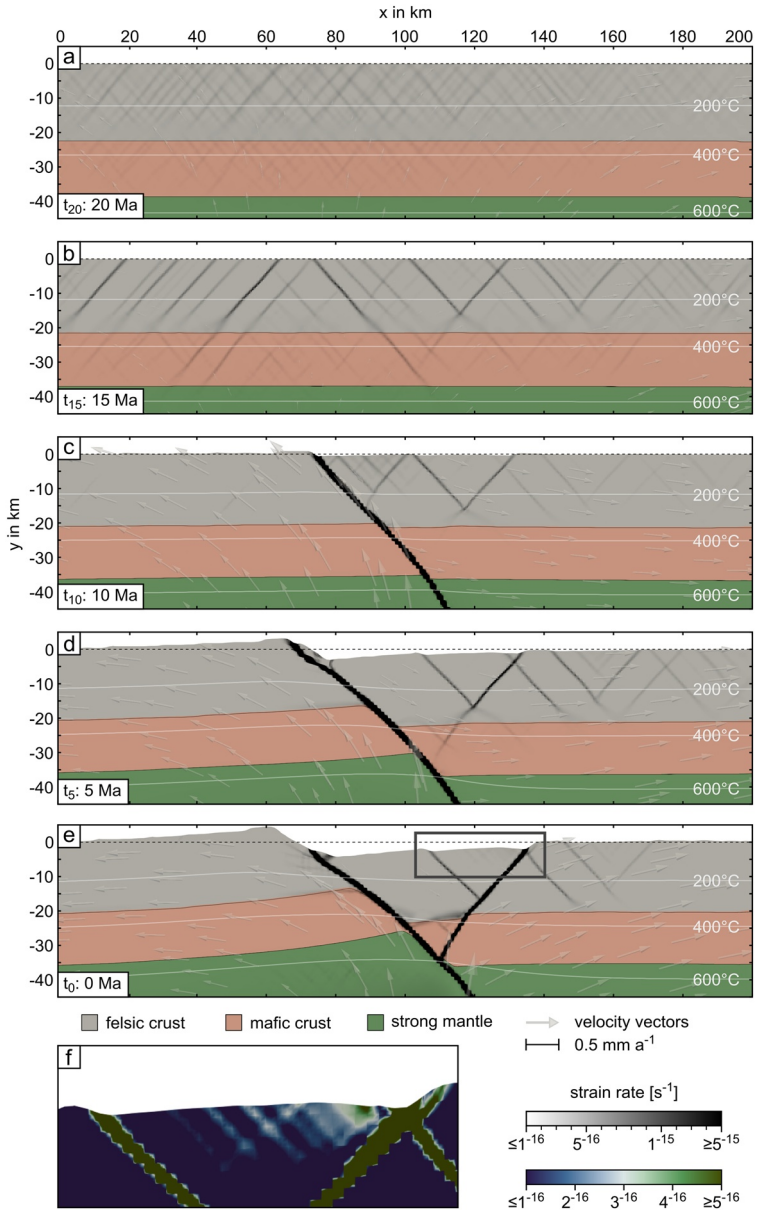

Figure 3. Evolution of the reference model. (a) Syn-rift phase immediately after prescribing the extension velocity of 2 mma^{-1} at the boundaries. The strain rate pattern originates from the seeded strain and the implemented friction softening. Model time identical to Figure 2c (b) Localization of deformation slowly increases in the competing fault network before onset of rifting. (c) Asymmetric onset of rifting, initial uplift of the main rift shoulder at 10 Ma. (d) Border fault localization at 5 Ma. (e) State of the rift that serves as our reference model for a comparison with the present-day Southern Kenya Rift. A westward dipping border fault has formed in the east, and shallow, crustal fault activity is observed in the eastern half of the graben. (f) Zoom of the upper crustal fault network.

comparing the models at the same modeled time, the results are compared after 10 million years of active rifting with the time of onset defined as the first occurrence of significant displacement along the main border fault(s). This way, the amount of deformation that is accommodated within the fault systems is more comparable. Note that the polarity of asymmetric faulting is random, but for the ease of visual inspection and comparison we mirrored model figures if necessary, such that the main border fault dips to the right (Figure 6).

In this numerical setup, we find that about 50% of the models are strongly asymmetric with one main border fault active after 10 million years of active rifting (*one-sided*, e.g., Figure 6 M1–M3). Flexural hang-

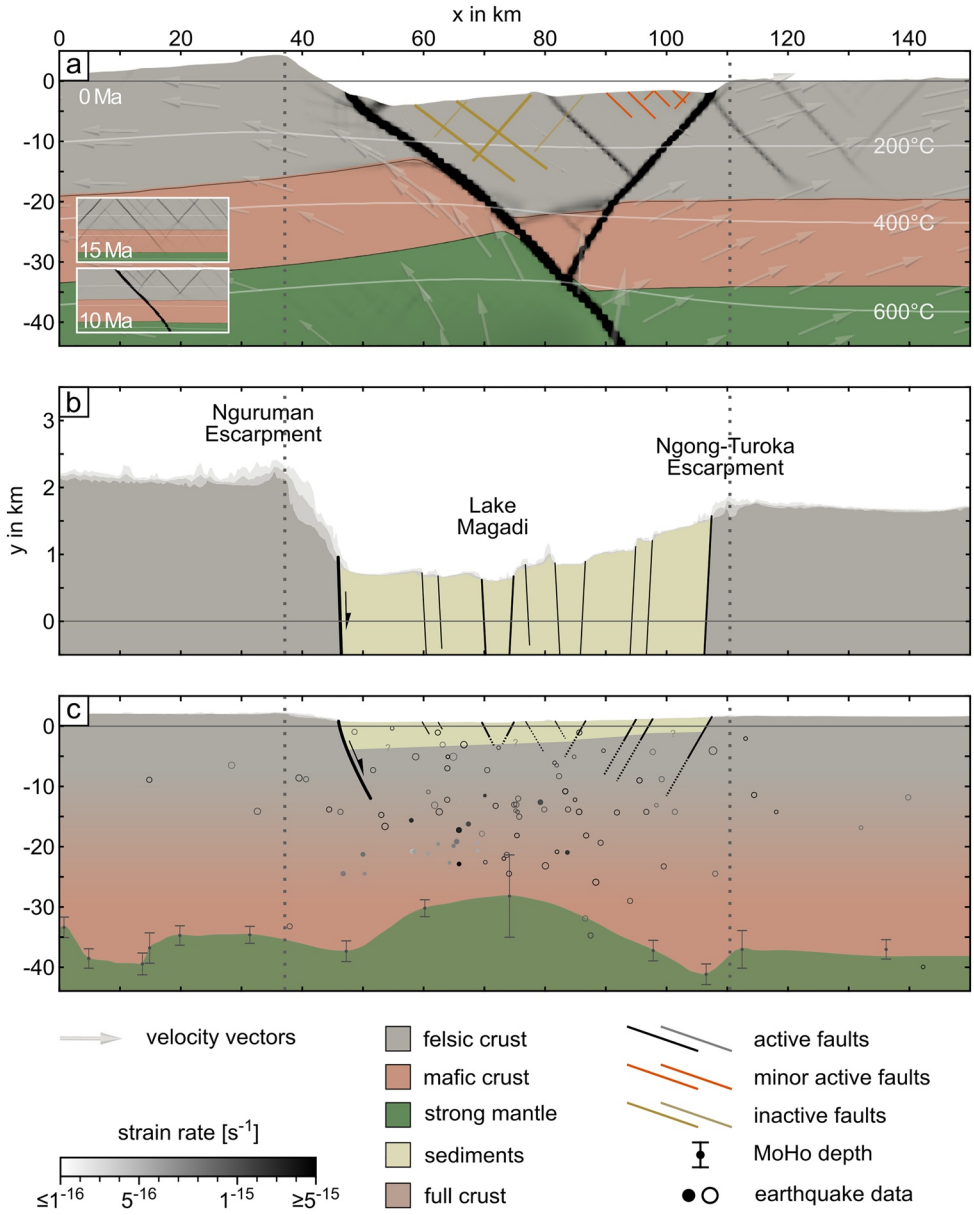

Figure 4. Comparison of the numerical model and an observational cross section of the Southern Kenya Rift. (a) Snapshot of the numerical model with active (black and red) and inactive (dark yellow) faults. (b) Topographic swath across the Southern Kenya Rift, based on the TanDEM-X digital elevation model (10 times vertical exaggeration). Dark, medium, and light gray indicate minimum, mean, and maximum topography along 5 km wide swath; profile location indicated in Figure 1b. Mapped faults based on Baker (1958). (c) Cross section with earthquake data (filled circles: Weinstein et al., 2017; open circles: Hollnack & Stangl, 1998), Moho-depth measurements (small dots with error bars: Plasman et al., 2017) and estimated sediment thicknesses (yellow: Birt et al., 1997).

ing-wall deformation is distributed over several secondary faults, with varying quantity and dip directions. We classify 40% of the models as *intermediate* such as our reference model (e.g., Figure 6 M4, MRef, M5). These models feature one dominant border fault, but secondary deformation in the hanging-wall is more pronounced than in the *one-sided* models. Only 10% of the models fall into the third, *two-sided* category (Figure 6 M6–M8), of which only one model (M6) features a symmetric border-fault geometry. All examples of this category feature a westward dipping border fault on the eastern rift side that reaches into the lithospheric mantle and limits the depth of the main fault in comparison to the more asymmetric models. Although models may be categorized at certain snapshots as in Figure 6, fault geometries actually develop

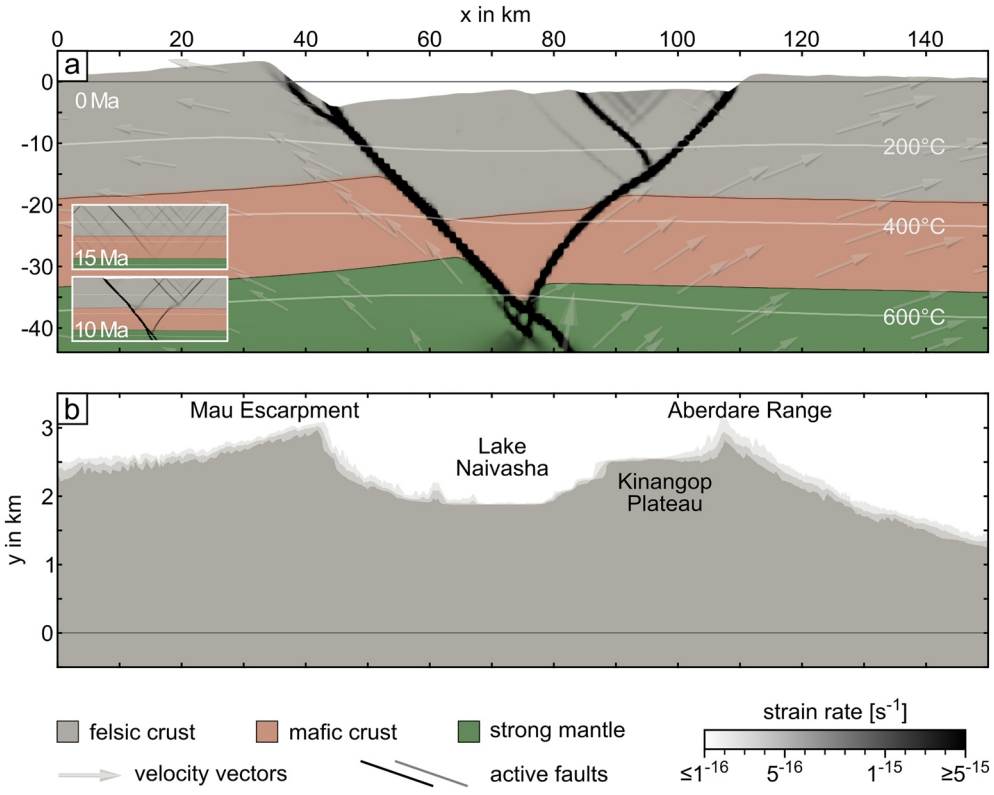

Figure 5. Comparison of a numerical model with the same setup as the reference model, but different random noise, and a cross section of the Central Kenya Rift. (a) Snapshot of the numerical model results. (b) Topographic swath profile of the Central Kenya Rift, based on the TanDEM-X digital elevation model (10 times vertical exaggeration). Dark, medium and light gray indicate minimum, mean and maximum topography along 5-km-wide swath; profile location indicated in Figure 1b.

over time. Strongly asymmetric models, for example, tend to become more symmetric due to coalescence of secondary faulting. In general, we find that the principal rift style (narrow) is unaffected by small-scale inheritance, but the tectonic history of each model may differ significantly. Deformation patterns are strongly influenced by the initial random noise distribution, especially in case of the hanging-wall segmentation and in the central area of normal fault blocks affecting the upper crust.

5. Discussion

Rifting in our models initiates across a distributed and complex network of low-deformation faults. Over time, the early developed fault network of individual faults coalesces into a system with a reduced number of faults that each accommodates larger displacements. This model evolution reproduces results of Cowie et al. (2005), who found that faults and shear zones that are characterized by a low maximum strain rate are active for a shorter time than faults with higher maximum strain rates. In agreement with our results, these authors explained the migration of fault activity into a narrower zone by a combination of crustal strain localization due to brittle failure and a co-evolving thermal structure. Our experimental results are in line with the observations from the Southern Kenya Rift, where after the formation of the first western border fault, hanging-wall flexure and a second phase of fault coalescence led to border-fault localization on the eastern rift side. The involved major crustal shear zones enable lithosphere-scale necking that strongly decreases the thickness of the lithosphere (Lavier & Manatschal, 2006).

Sustained and pronounced volcanic activity has been a major feature in all sectors of the Kenya Rift (Baker et al., 1971; Macdonald et al., 2001; Rooney, 2020; Williams, 1969b); however, we model rift evolution with a purely tectonic setup that does not account for diking or magmatic underplating. This apparent contradic-

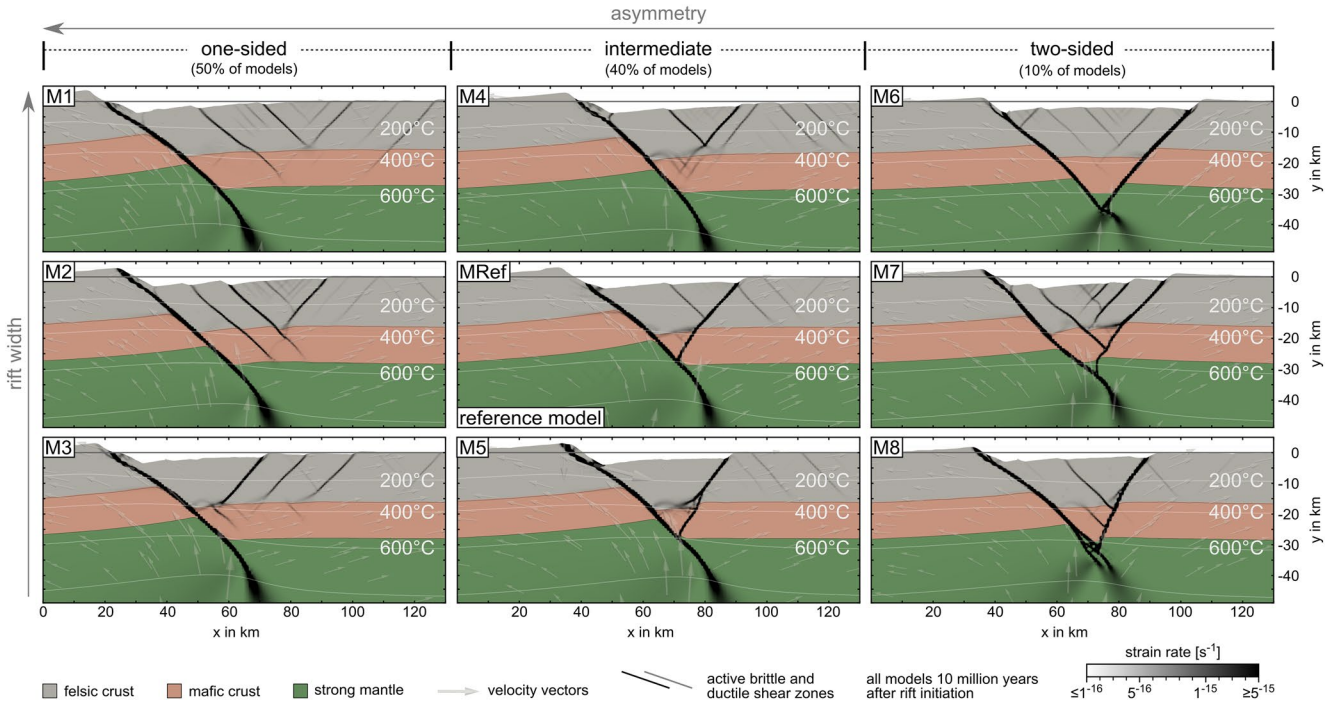

Figure 6. Impact of different random noise patterns on rift style. The only difference in the setup of the models is the randomized initial strain distribution. Combined with strain-dependent friction and viscous softening, individual fault networks develop in each model. About half of the models are strongly asymmetric (one-sided) with a dominant main border fault and distributed hanging-wall deformation with varying fault-dip directions (M1–M3). The second largest group (intermediate, ~40% of models) also features a main border fault, but deformation on the eastern rift border is more localized (M4, MRef, and M5). Two-sided models (M6–M8) constitute the smallest group (~10%). While M7 and M8 still feature an asymmetric fault geometry, M6 has symmetric border faults with similar displacements. Models M6–M8 are different from the other two groups and both have a pronounced eastern border fault that extends into the lithospheric mantle and connects to the main fault at depth.

tion is nevertheless justified when considering first-order features: the existence of important border faults, the Nguruman, Mau or Sattima faults, clearly illustrates that a large part of the extension is accommodated by faulting. Intra-basin faults, however, are likely affected by stress changes related to dike intrusion at depth (Behn et al., 2006; Rowland et al., 2007), providing a possible explanation for the second-order differences between our model and observations. Below we discuss these issues in more detail for the central and southern sectors of the Kenya Rift.

5.1. Southern Kenya Rift

We compare our numerical model to the available structural and stratigraphic data of the Southern Kenya Rift before we discuss the temporal evolution of the system in a second step. The first-order model geometry consisting of the main western border fault and a pronounced westward dipping fault in the east is in very good agreement with field and seismological observations (Figure 4). While the eastward-dipping border fault in our reference model features a high rift shoulder associated with a greater throw, the major fault on the eastern side of the rift valley records less displacement. From shoulder to shoulder, the rift is ~70 km wide, both in our experiment and in the Southern Kenya Rift. As in our model, a subdued area of high topography is observed in the basin center in nature and defined in both cases by a gentle westward-directed topographic gradient. In the model, the internal part of the eastern half of the rift is characterized by a shallow fault network in the top third of the upper crustal layer that may be responsible for producing the observed rift-parallel densely faulted rift center (Figure 3d). In nature, the thickness of the crystalline crust (i.e., excluding sedimentary cover) ranges between 25 and 30 km in the thinned rift center and up to 40 km in rift shoulder areas, and respective Moho depths range between 31 and 43 km relative to sea level (Birt, 1996; Birt et al., 1997; Dugda et al., 2005; Ebinger et al., 2017; Green et al., 1991; Tugume et al., 2012; Sippel et al., 2017). These values agree very well with the crustal thicknesses of 25–30 km beneath the rift

center and 40 km beneath the rift shoulders observed in the numerical model (see Figure 3e), particularly when considering that ~4–5 km of magmatic underplating can be expected in the Kenya rift (Thybo et al., 2000).

The evolution of the numerical model reproduces the asymmetric pattern of the overall rift evolution in southern Kenya. The first large-scale and unambiguous evidence for extensional tectonic activity is the formation of the eastward-dipping main border fault along the Nguruman Escarpment in South Kenya. The Nguruman fault is a major rift-bounding structure that is associated with an up to 40-m-wide cataclastic zone that follows the gneissic foliation in the basement rocks of the Mozambique Belt (Baker, 1958; Hetzel & Strecker, 1994). Stratigraphic relationships between Miocene nephelinites with an age range between ~15 and 9 Ma, the Nguruman fault scarp, and 6.9-million-year-old flood phonolites and trachytes that are banked against the fault scarp document that major faulting must have occurred here after 9 Ma and prior to 6.9 Ma (Baker, 1958; Baker & Mitchell, 1976; Crossley, 1979).

Conversely, on the eastern side of the rift our numerical model predicts a delay of 5 Ma (at t_5) in activity of the border-fault system due to the flexure of the central block (Figure 3d). This agrees with regional stratigraphic and structural relationships across the Ngong-Turoka escarpment on the eastern rift border, which also record a much later onset of the segmentation of a monocline that had formed in the ubiquitous Mio-Pliocene Trachytes (here, the 3.3-million-year-old Nairobi Trachyte), which ultimately formed a pronounced set of escarpments that now define the eastern rift flank (Baker et al., 1988). In addition, our model predicts continued tectonic subsidence along the Nguruman Escarpment during the hanging-wall segmentation at the eastern rift border. These model results are supported by geological observations at the Nguruman Escarpment, where lateral pinchouts and direct contacts of Pliocene flood basalts (3.1–2.3 Ma) with faults at the Nguruman Escarpment (i.e., Kirikiti Basalts, Crossley, 1979) document protracted faulting and the generation of topographic conditions that prevented the spillover of these lavas on the western rift-shoulder areas. Thus, as predicted in the model, Pliocene tectonic activity at both sides of the Southern Kenya Rift ultimately generated a full-graben stage with two conjugate border faults where all tectonic and volcanic activity has been confined until the present day ($t_{now} = 0$ Ma; Figures 3e and 4).

The valley floor of the Southern Kenya Rift is dissected by a densely spaced, N-S-to-NNE-striking fault array (Baker, 1958; Ibs-von Seht et al., 2001; Weinstein et al., 2017). These faults are characterized by an average density of 1.6 surface faults per kilometer, each showing a throw of at least 35 m (e.g., Baker, 1958). In general, it has been suggested that the spacing between adjacent normal faults is proportional to the thickness of the faulted layer (Dyksterhuis et al., 2007; Sharples et al., 2015). The dense fault spacing in the Southern Kenya Rift, however, cannot be related to the comparably thick brittle crust in this region (Albaric et al., 2009). In the model, the maximum depth of brittle faulting beneath the central basin is 5 km while the brittle-ductile transition is located at ~15 km depth (Figures 3f and 4a). These values correspond to earthquake-hypocenter depths and sectors of brittle deformation documented by an earthquake-recording network in the greater Lake Magadi region (Ibs-von Seht et al., 2001). Our model results explain the predicted high fault density through hanging-wall bending, which leads to significantly closer-spaced fault arrays than expected from brittle layer thickness (Figure 3f). This can be understood when considering that hanging-wall flexure causes tensional stresses and normal faulting (Bott, 1996) above the neutral plane of bending, which is much shallower than the brittle-ductile transition. Our model also shows that flexure takes place even after localization of the eastern border fault (Figure 3). This flexure of a hanging-wall block could explain the distributed intra-basin fault of the Magadi-Natron basin (Baker, 1958; Muirhead et al., 2016). An additional way to discriminate between normal faulting related to bending stresses in the hanging-wall block and regionally controlled extension may be achieved by analyzing fault-length distributions, since bending-related normal faults tend to deviate from the commonly observed power-law distribution of pure-shear normal faults (e.g., Supak et al., 2006). In this context, it is interesting that Muirhead et al. (2016) found that cumulative frequency plots of fault lengths within the Magadi-Natron basin are slightly more compatible with an exponential fit rather than a power-law fit, which suggests that the faults in the Magadi-Natron basin may reflect flexure-induced, shallow normal faulting. However, we caution that these densely spaced normal faults could alternatively be related to locally elevated tensional stresses due to shallow dike emplacement (Behn et al., 2006; Muirhead et al., 2016; Rowland et al., 2007), a process that we cannot reproduce with our current modeling capabilities. While a certain fraction of normal faults in

the Kenya Rift may be associated with dike emplacement (e.g., Ibs-van Seht et al., 2001; Tongue et al., 1992), we speculate that such a process should have a greater impact in more advanced regions of extension, such as Afar, where the magmatic input is significantly larger than in our study region (Kendall et al., 2005; Stab et al., 2015; Wright et al., 2006).

The spatial distribution of extension within the Southern Kenya Rift has been recently quantified by means of analyzing fault systems, GPS-based motion vectors, and the chronology of lava-flow emplacement (Muirhead et al., 2016). The authors infer that 0.4–0.66 mm a^{-1} is accommodated by slip along the Nguruman border fault on the western rift side while 1.34–1.60 mm a^{-1} is taken up by the intra-rift faults. Our reference model for the Southern Kenya Rift exhibits 1.0 mm a^{-1} for the western border fault, 0.44 mm a^{-1} across the eastern border fault, and 0.1 mm for intra-basin faults. The remaining 0.46 mm a^{-1} is accommodated by deformation outside the rift, mostly along faults east of the eastern border faults. In particular, deformation in the modeled rift center does not match the extension values across the small-scale intra-rift fault network of Muirhead et al. (2016). We speculate that this might be due to insufficient numerical representation of magmatic weakening processes acting in the rift. These processes include (1) thermal weakening of the crust due to magmatic addition (Thybo et al., 2000), (2) dike injections that drive extension (Buck, 2006; Oliva et al., 2019) and near-surface faulting (Behn et al., 2006), and (3) fluid flow along rift-internal faults (Muirhead et al., 2016), which reduces the effective friction on faults. By forcing deformation to the rift center, these weakening processes would ultimately reduce activity of the border faults. Future comparative modeling studies should therefore set out to consider magmatic processes associated with diking and fluid migration in order to investigate their role in localization processes within young continental rift settings at lithospheric-scale.

5.2. Central Kenya Rift

Our model predicts asymmetric rift initiation with an east-dipping normal fault along the future western side of the rift. This is supported by the geological observations and the distribution of regionally extensive Middle Miocene Plateau Phonolite flows emplaced prior to the onset of faulting on the western side of the rift (Baker et al., 1971, 1988; Strecker et al., 1990). The numerical model chosen for comparison with the Central Kenya Rift (Figure 5a) is similar to the reference model of the Southern Kenya Rift (Section 4.2), but it differs in the displacement along the secondary (eastern) border fault that develops ~5 Ma after rift initiation a difference that is solely caused by an alternative random noise pattern in initial strain. This compares, very well with geological interpretations where spatially more restricted emplacement of lava flows within the developing rift basin and the overspilling of flows toward the east in the area of the present-day rift shoulders supports the notion of an initial half-graben, followed by segmentation of the hanging-wall block between 5.5 and 4 Ma (Baker et al., 1988; Clarke et al., 1990; Shackleton, 1945).

Further similarities exist between our Central Kenya Rift model (Figure 5a) and interpretations drawn from stratigraphic relationships and faulting on the western side of the central segment, where our model predicts a 4-km-offset of the crystalline basement surface. This can also be inferred from field-based observations and data from geothermal drilling in the Naivasha area (Clarke et al., 1990; Strecker, 1991) indicating that the throw involving the Mio-Pliocene Plateau Trachytes is on the order of 2 km since ~3 Ma. In addition, the total offset of the basement rocks based on exposures on the western rift shoulder and their depth position obtained from seismic refraction data (KRISP Working Group, 1987) is ~4 km (Strecker, 1991). However, the formation of the Kinangop Plateau (Figure 5), limited by the westward-dipping Sattima fault in the east and the westward-dipping Kinangop fault to the west, is not represented in the numerical model. Instead, a synthetic normal fault has developed in our model that segments the hanging-wall block.

5.3. Influence of Inheritance and Crustal Anisotropies

Our analysis shows that the initial fault pattern may strongly control the first-order structure of a rift. In some cases, the initial fault configuration may even override the rheologically expected symmetry (Huismans et al., 2005) and induce a symmetric rift in a setup that otherwise generates predominantly asymmetric geometries (Figure 6). This means that any process affecting the initial fault configuration, such

as rupture propagation along structures inherited from earlier deformation phases (Muirhead & Kattenhorn, 2018), strain softening (Huismans & Beaumont, 2003) or initial diking (Buck, 2006) may affect the first-order structural evolution of a rift and possibly of the future rifted margin.

In the lithosphere below the Kenya Rift, the Late Proterozoic Mozambique Belt is a known major crustal heterogeneity that once constituted a collisional orogen in the suture zone between East and West Gondwana (Smith & Mosley, 1993), and it is hypothesized to have influenced the geometry of the Kenya Rift during all stages of its evolution (e.g., Hetzel & Strecker, 1994; Muirhead & Kattenhorn, 2018; Robertson et al., 2015; Shackleton, 1976; Shackleton & Ries, 1984; Smith, 1994; Smith & Mosley, 1993). Our model sheds new light on the influence of such crustal heterogeneities: while most numerical models change rheological setup and strain softening parameters (e.g., Armitage et al., 2018; Brune et al., 2017b; Duclaux et al., 2020; Ros et al., 2017), we varied the initial random strain pattern and kept rheology and strain softening the same. By using this approach, we are able to show that low-degree variability of crustal strength may decisively influence rift geometry. While predominantly asymmetric rift configurations can be generated in this way, in some cases, variability in crustal strength may even lead to symmetric rift patterns in a cold and brittle lithosphere (Figure 6).

6. Conclusions

In this study, we employed a 2D numerical model to integrate geological and geophysical data into a framework that enables us to explain the tectonically characteristic evolution of the Southern and Central Kenya Rift. This encompasses the following processes and steps: (1) a broad zone of low deformation and competing faults develops until coalescence of faults takes place and a single border fault localizes before (2) a conjugate border fault forms and (3) an anomalously shallow fault network emerges due to bending of the central hanging-wall block. Even though volcanic activity is ubiquitous in the Kenya Rift, our purely tectonic model is capable of reproducing first-order characteristics of the rift. By utilizing a random noise implementation of initial strain, we highlight that the 2D setup is capable of addressing along-strike variations of the rift, but also that small-scale crustal inheritance strongly affects first-order faults and overall rift geometry.

Data Availability Statement

All data that this numerical study is based on can be found in Table 1 and Figure 2 and is referenced in corresponding captions. Figures were created using Paraview and Matlab and color maps were taken from Crameri (2018). Elevation data shown in Figures 1, 4 and 5 are based on the TanDEM-X science DEM, granted by the German Space Agency (© DLR 2017).

Acknowledgments
This study was conducted within the Helmholtz Young Investigators Group CRYSTALS (VH-NG-1132). We thank the Computational Infrastructure for Geodynamics (geodynamics.org), which is funded by the National Science Foundation under award EAR-0949446 and EAR-1550901 for supporting the development of ASPECT. MR and SR acknowledge field support by R. Potts, Smithsonian Institution, Washington DC and Geothermal Development Company, Kenya, and discussions with L. Olaka, University of Nairobi. The work was supported by the North-German Supercomputing Alliance (HLRN). We thank reviewers James Muirhead, Jolante van Wijk, and Anthony Jourdon as well as Associate Editor Luc Lavier for detailed and very constructive comments that significantly helped to improve this manuscript.
Open access funding enabled and organized by Projekt DEAL.

References

Albaric, J., Déverchère, J., Petit, C., Perrot, J., & Le Gall, B. (2009). Crustal rheology and depth distribution of earthquakes: Insights from the central and southern East African Rift System. *Tectonophysics*, *468*(1–4), 28–41.

Armitage, J. J., Petersen, K. D., & Pérez-Gussinyé, M. (2018). The role of crustal strength in controlling magmatism and melt chemistry during rifting and breakup. *Geochemistry, Geophysics, Geosystems*, *19*(2), 534–550. https://doi.org/10.1002/2017GC007326

Atmaoui, N., & Hollnack, D. (2003). Neotectonics and extension direction of the Southern Kenya Rift, Lake Magadi area. *Tectonophysics*, *364*(1–2), 71–83. https://doi.org/10.1016/S0040-1951(03)00051-9

Baker, B. H. (1958). *Geological Survey of Kenya, Geology of the Magadi Area, degree sheet 51, SW Quarter (No. 42)*. Geological Survey of Kenya Report.

Baker, B. H., & Mitchell, J. G. (1976). Volcanic stratigraphy and geochronology of the Kedong-Olorgesailie area and the evolution of the South Kenya rift valley. *Journal of the Geological Society*, *132*(5), 467–484.

Baker, B. H., Mitchell, J. G., & Williams, L. A. J. (1988). Stratigraphy, geochronology and volcano-tectonic evolution of the Kedong-Naivasha-Kinangop region, Gregory Rift Valley, Kenya. *Journal of the Geological Society*, *145*(1), 107–116.

Baker, B. H., Williams, L. A. J., Miller, J. A., & Fitch, F. J. (1971). Sequence and geochronology of the Kenya rift volcanics. *Tectonophysics*, *11*(3), 191–215. https://doi.org/10.1016/0040-1951(71)90030-8

Bangerth, W., Austermann, J., Bürg, M., Cox, S., Durkin, W., Euen, G., et al. (2019). *ASPECT: Advanced Solver for Problems in Earth's ConvecTion, User Manual*. Figshare. https://doi.org/10.6084/m9.figshare.4865333

Bangerth, W., Dannberg, J., Gassmoeller, R., & Heister, T. (2018). *Aspect V2.0.1*. Zenodo. https://doi.org/10.5281/zenodo.1297145

Bassi, G. (1991). Factors controlling the style of continental rifting: Insights from numerical modeling. *Earth and Planetary Science Letters*, *105*(4), 430–452. https://doi.org/10.1016/0012-821X(91)90183-I

Bastow, I. D., & Keir, D. (2011). The protracted development of the continent-ocean transition in Afar. *Nature Geoscience*, *4*(4), 248–250. https://doi.org/10.1038/ngeo1095

Behn, M., Buck, W., & Sacks, I. (2006). Topographic controls on dike injection in volcanic rift zones. *Earth and Planetary Science Letters*, *246*(3), 188–196. https://doi.org/10.1016/j.epsl.2006.04.005

Beniest, A., Koptev, A., & Burov, E. (2017). Numerical models for continental break-up: Implications for the South Atlantic. *Earth and Planetary Science Letters*, *461*, 176–189. https://doi.org/10.1016/j.epsl.2016.12.034

Beutel, E., van Wijk, J., Ebinger, C., Keir, D., & Agostini, A. (2010). Formation and stability of magmatic segments in the Main Ethiopian and Afar rifts. *Earth and Planetary Science Letters*, *293*(3–4), 225–235. https://doi.org/10.1016/j.epsl.2010.02.006

Birt, C. S. (1996). Geophysical investigation of active continental rifting in southern Kenya (Doctoral dissertation). University of Leicester. Retrieved from https://hdl.handle.net/2381/34979

Birt, C. S., Maguire, P. K. H., Khan, M. A., Thybo, H., Keller, G. R., & Patel, J. (1997). The influence of pre-existing structures on the evolution of the southern Kenya Rift Valley—evidence from seismic and gravity studies. *Tectonophysics*, *278*(1–4), 211–242. https://doi.org/10.1016/S0040-1951(97)00105-4

Bott, M. H. P. (1996). Flexure associated with planar faulting. *Geophysical Journal International*, *126*(3), F21–F24. https://doi.org/10.1111/j.1365-246X.1996.tb04692.x

Brun, J. P. (1999). Narrow rifts versus wide rifts: Inferences for the mechanics of rifting from laboratory experiments. *Philosophical Transactions of the Royal Society of London, Series A: Mathematical, Physical and Engineering Sciences*, *357*(1753), 695–712. https://doi.org/10.1098/rsta.1999.0349

Brune, S. (2014). Evolution of stress and fault patterns in oblique rift systems: 3-D numerical lithospheric-scale experiments from rift to breakup. *Geochemistry, Geophysics, Geosystems*, *15*(8), 3392–3415. https://doi.org/10.1002/2014GC005446

Brune, S., Corti, G., & Ranalli, G. (2017a). Controls of inherited lithospheric heterogeneity on rift linkage: Numerical and analog models of interaction between the Kenyan and Ethiopian rifts across the Turkana depression. *Tectonics*, *36*(9), e2017TC004739. https://doi.org/10.1002/2017TC004739

Brune, S., Heine, C., Clift, P. D., & Pérez-Gussinyé, M. (2017b). Rifted margin architecture and crustal rheology: Reviewing Iberia-Newfoundland, Central South Atlantic, and South China Sea. *Marine and Petroleum Geology*, *79*, 257–281. https://doi.org/10.1016/j.marpetgeo.2016.10.018

Brune, S., Heine, C., Perez-Gussinye, M., & Sobolev, S. V. (2014). Rift migration explains continental margin asymmetry and crustal hyper-extension. *Nature Communications*, *5*(4014). https://doi.org/10.1038/ncomms5014

Buck, W. R. (2006). The role of magma in the development of the Afro-Arabian Rift System. *Geological Society, London, Special Publications*, *259*(1), 43–54. https://doi.org/10.1144/GSL.SP.2006.259.01.05

Buck, W. R., Lavier, L. L., & Poliakov, A. N. B. (1999). How to make a rift wide. *Philosophical Transactions of the Royal Society of London, Series A: Mathematical, Physical and Engineering Sciences*, *357*(1753), 671–693. https://doi.org/10.1098/rsta.1999.0348

Buck, W. R., Lavier, L. L., & Poliakov, A. N. B. (2005). Modes of faulting at mid-ocean ridges. *Nature*, *434*(7034), 719–723. https://doi.org/10.1038/nature03358

Buiter, S. J. H., Huismans, R. S., & Beaumont, C. (2008). Dissipation analysis as a guide to mode selection during crustal extension and implications for the styles of sedimentary basins. *Journal of Geophysical Research*, *113*(B6). https://doi.org/10.1029/2007JB005272

Bunge, H.-P. (2005). Low plume excess temperature and high core heat flux inferred from non-adiabatic geotherms in internally heated mantle circulation models. *Physics of the Earth and Planetary Interiors*, *153*(1–3), 3–10. https://doi.org/10.1016/j.pepi.2005.03.017

Burov, E., & Schubert, G. (2007). Plate rheology and mechanics. In *Treatise on Geophysics: Crust and lithosphere dynamics* (Vol. 6, pp. 99–151). https://doi.org/10.1016/b978-044452748-6/00102-4

Cacace, M., & Scheck-Wenderoth, M. (2016). Why intracontinental basins subside longer: 3-D feedback effects of lithospheric cooling and sedimentation on the flexural strength of the lithosphere. *Journal of Geophysical Research: Solid Earth*, *121*(5), 3742–3761. https://doi.org/10.1002/2015JB012682

Calais, E., d'Oreye, N., Albaric, J., Deschamps, A., Delvaux, D., Déverchère, J., et al. (2008). Strain accommodation by slow slip and dyking in a youthful continental rift, East Africa. *Nature*, *456*(7223), 783–787. https://doi.org/10.1038/nature07478

Celli, N. L., Lebedev, S., Schaeffer, A. J., & Gaina, C. (2020). African cratonic lithosphere carved by mantle plumes. *Nature Communications*, *11*(1), 92. https://doi.org/10.1038/s41467-019-13871-2

Chapman, G. R., & Brook, M. (1978). Chronostratigraphy of the Baringo Basin, Kenya. *Geological Society, London, Special Publications*. https://doi.org/10.1144/GSL.SP.1978.006.01.16

Civiero, C., Armitage, J. J., Goes, S., & Hammond, J. O. S. (2019). The Seismic Signature of Upper-Mantle Plumes: Application to the Northern East African Rift. *Geochemistry, Geophysics, Geosystems*, *20*(12), 6106–6122. https://doi.org/10.1029/2019GC008636

Civiero, C., Hammond, J. O. S., Goes, S., Fishwick, S., Ahmed, A., Ayele, A., et al. (2015). Multiple mantle upwellings in the transition zone beneath the northern East- African Rift system from relative P-wave travel-time tomography. *Geochemistry, Geophysics, Geosystems*, *16*(9), 2949–2968. https://doi.org/10.1002/2015GC005948

Clarke, M. C. G., Woodhall, D. G., Allen, D., & Darling, G. (1990). *Geological, volcanological and hydrological controls on the occurrence of geothermal activity in the area surrounding Lake Naivasha, Kenya*. Kenya. Nairobi, Kenya: Ministry of Energy Report.

Corti, G. (2009). Continental rift evolution: From rift initiation to incipient break-up in the Main Ethiopian Rift, East Africa. *Earth-Science Reviews*, *96*(1–2), 1–53. https://doi.org/10.1016/j.earscirev.2009.06.005

Corti, G. (2012). Evolution and characteristics of continental rifting: Analog modeling-inspired view and comparison with examples from the East African Rift System. *Tectonophysics*, *522–523*, 1–33. https://doi.org/10.1016/j.tecto.2011.06.010

Corti, G., Cioni, R., Franceschini, Z., Sani, F., Scaillet, S., Molin, P., et al. (2019). Aborted propagation of the Ethiopian rift caused by linkage with the Kenyan rift. *Nature Communications*, *10*(1), 1309. https://doi.org/10.1038/s41467-019-09335-2

Corti, G., van Wijk, J., Bonini, M., Sokoutis, D., Cloetingh, S., Innocenti, F., & Manetti, P. (2003). Transition from continental break-up to punctiform seafloor spreading: How fast, symmetric and magmatic. *Geophysical Research Letters*, *30*(12), 1604. https://doi.org/10.1029/2003GL017374

Corti, G., van Wijk, J., Cloetingh, S., & Morley, C. K. (2007). Tectonic inheritance and continental rift architecture: Numerical and analogue models of the East African Rift system. *Tectonics*, *26*(6). https://doi.org/10.1029/2006TC002086

Cowie, P., Underhill, J., Behn, M., Lin, J., & Gill, C. (2005). Spatio-temporal evolution of strain accumulation derived from multi-scale observations of Late Jurassic rifting in the northern North Sea: A critical test of models for lithospheric extension. *Earth and Planetary Science Letters*, *234*(3–4), 401–419. https://doi.org/10.1016/j.epsl.2005.01.039

Crameri, F. (2018). Geodynamic diagnostics, scientific visualisation and StagLab 3.0. *Geoscientific Model Development Discussions*, 1–41. https://doi.org/10.5194/gmd-2017-328

Crossley, R. (1979). The Cenozoic stratigraphy and structure of the western part of the Rift Valley in southern Kenya. *Journal of the Geological Society*, *136*(4), 393–405. https://doi.org/10.1144/gsjgs.136.4.0393

Delvaux, D., Kervyn, F., Macheyeki, A. S., & Temu, E. B. (2012). Geodynamic significance of the TRM segment in the East African Rift (W-Tanzania): Active tectonics and paleostress in the Ufipa plateau and Rukwa basin. *Journal of Structural Geology*, *37*, 161–180. https://doi.org/10.1016/j.jsg.2012.01.008

Döhmann, M. J. E. A., Brune, S., Nardini, L., Rybacki, E., & Dresen, G. (2019). Strain Localization and Weakening Processes in Viscously Deforming Rocks: Numerical Modeling Based on Laboratory Torsion Experiments. *Journal of Geophysical Research: Solid Earth*, *124*(1), 1120–1137. https://doi.org/10.1029/2018JB016917

Duclaux, G., Huismans, R. S., & May, D. A. (2020). Rotation, narrowing, and preferential reactivation of brittle structures during oblique rifting. *Earth and Planetary Science Letters*, *531*, 115952. https://doi.org/10.1016/j.epsl.2019.115952

Dugda, M. T., Nyblade, A. A., Julia, J., Langston, C. A., Ammon, C. J., & Simiyu, S. (2005). Crustal structure in Ethiopia and Kenya from receiver function analysis: Implications for rift development in eastern Africa. *Journal of Geophysical Research*, *110*(B1). https://doi.org/10.1029/2004JB003065

Duretz, T., Petri, B., Mohn, G., Schmalholz, S. M., Schenker, F. L., & Müntener, O. (2016). The importance of structural softening for the evolution and architecture of passive margins. *Scientific Reports*, *6*, 38704.

Dyksterhuis, S., Rey, P., Müller, R. D., Moresi, L., Ebinger, C., & Scholz, C. A. (2007). Effects of initial weakness on rift architecture continental rift basins: The East African perspective. *Geological Society, London, Special Publications, Tectonics of sedimentary basins: Recent advances*, *282*(1), 443–455. https://doi.org/10.1002/9781444347166.ch9

Ebinger, C., & Scholz, C. A. (2011). Continental Rift Basins: The East African Perspective. In C. Busby & A. Azor (Eds.), *Tectonics of Sedimentary Basins*, 183–208. Chichester, UK: John Wiley & Sons.

Ebinger, C. J., Keir, D., Bastow, I. D., Whaler, K., Hammond, J. O. S., Ayele, A., et al. (2017). Crustal structure of active deformation zones in Africa: Implications for global crustal processes. *Tectonics*, *36*(12), 3298–3332. https://doi.org/10.1002/2017TC004526

Ego, J. K. (1994). *Sedimentology and diagenesis of Neogene sediments in the Central Kenya Rift Valley (MSc thesis)*,. Saskatoon: University of Saskatchewan. Retrieved from http://hdl.handle.net/10388/etd-01082010-110639

Faccenna, C., Glišović, P., Forte, A., Becker, T. W., Garzanti, E., Sembroni, A., & Gvirtzman, Z. (2019). Role of dynamic topography in sustaining the Nile River over 30 million years. *Nature Geoscience*, *12*(12), 1012–1017. https://doi.org/10.1038/s41561-019-0472-x

Gassmöller, R., Lokavarapu, H., Heien, E., Puckett, E. G., & Bangerth, W. (2018). Flexible and scalable particle-in-cell methods with adaptive mesh refinement for geodynamic computations. *Geochemistry, Geophysics, Geosystems*, *19*(9), 3596–3604. https://doi.org/10.1029/2018GC007508

Gawthorpe, R. L., & Leeder, M. R. (2008). Tectono-sedimentary evolution of active extensional basins. *Basin Research*, *12*(3-4), 195–218. https://doi.org/10.1111/j.1365-2117.2000.00121.x

Geological map of Kenya, with structural contours. Nairobi: Ministry of Energy and Regional Development of Kenya.

Gerbi, C., Culshaw, N., & Marsh, J. (2010). Magnitude of weakening during crustal-scale shear zone development. *Journal of Structural Geology*, *32*(1), 107–117. https://doi.org/10.1016/j.jsg.2009.10.002

Glerum, A., Brune, S., Stamps, D. S., & Strecker, M. R. (2020). Victoria continental microplate dynamics controlled by the lithospheric strength distribution of the East African Rift. *Nature Communications*, *11*(1), 2881. https://doi.org/10.1038/s41467-020-16176-x

Glerum, A., Thieulot, C., Fraters, M., Blom, C., & Spakman, W. (2018). Nonlinear viscoplasticity in ASPECT: Benchmarking and applications to subduction. *Solid Earth*, *9*(2), 267–294. https://doi.org/10.5194/se-9-267-2018

Green, W. V., Achauer, U., & Meyer, R. P. (1991). A three-dimensional seismic image of the crust and upper mantle beneath the Kenya rift. *Nature*, *354*(6350), 199–203. https://doi.org/10.1038/354199a0

Guth, A. (2014). *Maps of the southern Kenya rift*. Geological Society of America. https://doi.org/10.1130/2014.DMCH016

Hackman, B. D. (1988). Geology of the Baringo-Laikipia area, Republic of Kenya. *Ministry of Environmental and Natural Resources, Geology and Mines Department* Report No. 104.

Halldórsson, S. A., Hilton, D. R., Scarsi, P., Abebe, T., & Hopp, J. (2014). A common mantle plume source beneath the entire East African rift system revealed by coupled helium-neon systematics. *Geophysical Research Letters*, *41*(7), 2304–2311. https://doi.org/10.1002/2014GL059424

Hautot, S., Tarits, P., Whaler, K., Le Gall, B., Tiercelin, J.-J., & Le Turdu, C. (2000). Deep structure of the Baringo Rift Basin (central Kenya) from three-dimensional magnetotelluric imaging: Implications for rift evolution. *Journal of Geophysical Research*, *105*(B10), 23493–23518. https://doi.org/10.1029/2000JB900213

Heckenbach, E. L., Brune, S., Glerum, A. C., & Bott, J. (2021). Is There a speed limit for the thermal steady-state assumption in continental rifts? *Geochemistry, Geophysics, Geosystems*, *22*(3), e2020GC009577. https://doi.org/10.1029/2020GC009577

Heister, T., Dannberg, J., Gassmöller, R., & Bangerth, W. (2017). High accuracy mantle convection simulation through modern numerical methods - II: Realistic models and problems. *Geophysical Journal International*, *210*(2), 833–851. https://doi.org/10.1093/gji/ggx195

Hetzel, R., & Strecker, M. R. (1994). Late Mozambique Belt structures in western Kenya and their influence on the evolution of the Cenozoic Kenya Rift. *Journal of Structural Geology*, *16*(2), 189–201. https://doi.org/10.1016/0191-8141(94)90104-x

Hillaire-Marcel, C., Carro, O., & Casanova, J. (1986). 14C and Th/U dating of Pleistocene and Holocene stromatolites from East African paleolakes. *Quaternary Research*, *25*(3), 312–239. https://doi.org/10.1016/0033-5894(86)90004-9

Hirth, G., & Kohlstedt, D. (2003). Rheology of the upper mantle and the mantle wedge: A view from the experimentalists. *Geophysical Monograph Series*, *138*, 83–105. https://doi.org/10.1029/138GM06

Hodge, M., Fagereng, Å., Biggs, J., & Mdala, H. (2018). Controls on Early-Rift Geometry: New Perspectives From the Bilila-Mtakataka Fault, Malawi. *Geophysical Research Letters*, *45*(9), 3896–3905. https://doi.org/10.1029/2018GL077343

Hofmann, C., Courtillot, V., Féraud, G., Rochette, P., Yirgu, G., Ketefo, E., & Pik, R. (1997). Timing of the Ethiopian flood basalt event and implications for plume birth and global change. *Nature*, *389*(6653), 838–841. https://doi.org/10.1038/39853

Hollnack, D., & Stangl, R. (1998). The seismicity related to the southern part of the Kenya Rift. *Journal of African Earth Sciences*, *26*(3), 477–495. https://doi.org/10.1016/S0899-5362(98)00027-X

Huismans, R. S., & Beaumont, C. (2003). Symmetric and asymmetric lithospheric extension: Relative effects of frictional-plastic and viscous strain softening. *Journal of Geophysical Research*, *108*(B10). https://doi.org/10.1029/2002JB002026

Huismans, R. S., & Beaumont, C. (2011). Depth-dependent extension, two-stage breakup and cratonic underplating at rifted margins. *Nature*, *473*(7345), 74–78. https://doi.org/10.1038/nature09988

Huismans, R. S., Buiter, S. J. H., & Beaumont, C. (2005). Effect of plastic-viscous layering and strain softening on mode selection during lithospheric extension. *Journal of Geophysical Research*, *110*(B2). https://doi.org/10.1029/2004JB003114

Ibs-von Seht, M., Blumenstein, S., Wagner, R., Hollnack, D., & Wohlenberg, J. (2001). Seismicity, seismotectonics and crustal structure of the southern Kenya Rift-new data from the Lake Magadi area. *Geophysical Journal International*, *146*(2), 439–453. https://doi.org/10.1046/j.0956-540x.2001.01464.x

Jammes, S., & Lavier, L. L. (2019). Effect of contrasting strength from inherited crustal fabrics on the development of rifting margins. *Geosphere*. https://doi.org/10.1130/GES01686.1

Jaupart, C., Mareschal, J.-C., & Iarotsky, L. (2016). Radiogenic heat production in the continental crust. *Lithos*, *262*, 398–427. https://doi.org/10.1016/j.lithos.2016.07.017

Jeanniot, L., & Buiter, S. J. H. (2018). A quantitative analysis of transtensional margin width. *Earth and Planetary Science Letters*, *491*, 95–108. https://doi.org/10.1016/j.epsl.2018.03.003

Jourdon, A., Kergaravat, C., Duclaux, G., & Huguen, C. (2021). Looking beyond kinematics: 3D thermo-mechanical modeling reveals the dynamic of transform margins. *Solid Earth Discussions*, 1–34. https://doi.org/10.5194/se-2021-18

Katumwehe, A. B., Abdelsalam, M. G., & Atekwana, E. A. (2015). The role of pre-existing Precambrian structures in rift evolution: The Albertine and Rhino grabens, Uganda. *Tectonophysics*, *646*, 117–129. https://doi.org/10.1016/j.tecto.2015.01.022

Kendall, J.-M., & Lithgow-Bertelloni, C. (2016). Why is Africa rifting? *Geological Society, London, Special Publications*, *420*(1), 11–30. https://doi.org/10.1144/SP420.17

Kendall, J.-M., Stuart, G. W., Ebinger, C. J., Bastow, I. D., & Keir, D. (2005). Magma-assisted rifting in Ethiopia. *Nature*, *433*(7022), 146–148. https://doi.org/10.1038/nature03161

Khalil, H. M., Capitanio, F. A., Betts, P. G., & Cruden, A. R. (2020). 3-D analog modeling constraints on rifting in the Afar region. *Tectonics*, *39*(10), e2020TC006339. https://doi.org/10.1029/2020TC006339

Koptev, A., Burov, E., Gerya, T., Le Pourhiet, L., Leroy, S., Calais, E., & Jolivet, L. (2018). Plume-induced continental rifting and break-up in ultra-slow extension context: Insights from 3D numerical modeling. *Tectonophysics*, *746*, 121–137. https://doi.org/10.1016/j.tecto.2017.03.025

Koptev, A., Calais, E., Burov, E., Leroy, S., & Gerya, T. (2015). Dual continental rift systems generated by plume-lithosphere interaction. *Nature Geoscience*, *8*(5), 388–392. https://doi.org/10.1038/ngeo2401

KRISP Working Group. (1987). Structure of the Kenya rift from seismic refraction. *Nature*, *325*(6101), 239–242. https://doi.org/10.1038/325239a0

Kronbichler, M., Heister, T., & Bangerth, W. (2012). High accuracy mantle convection simulation through modern numerical methods. *Geophysical Journal International*, *191*(1), 12–29. https://doi.org/10.1111/j.1365-246X.2012.05609.x

Lavier, L. L., & Manatschal, G. (2006). A mechanism to thin the continental lithosphere at magma-poor margins. *Nature*, *440*(March), 324–328. https://doi.org/10.1038/nature04608

Lee, H., Muirhead, J. D., Fischer, T. P., Ebinger, C. J., Kattenhorn, S. A., Sharp, Z. D., & Kianji, G. (2016). Massive and prolonged deep carbon emissions associated with continental rifting. *Nature Geoscience*, *9*(2), 145–149. https://doi.org/10.1038/ngeo2622

Lenardic, A., Moresi, L., & Mühlhaus, H. (2000). The role of mobile belts for the longevity of deep cratonic lithosphere: The Crumple Zone Model. *Geophysical Research Letters*, *27*(8), 1235–1238. https://doi.org/10.1029/1999GL008410

Lippard, S. J. (1973). The petrology of phonolites from the Kenya Rift. *Lithos*, *6*(3), 217–234. https://doi.org/10.1016/0024-4937(73)90083-2

Macdonald, R., Rogers, N. W., Fitton, J. G., Black, S., & Smith, M. (2001). Plume-lithosphere interactions in the generation of the Basalts of the Kenya Rift, East Africa. *Journal of Petrology*, *42*(5), 877–900. https://doi.org/10.1093/petrology/42.5.877

Macgregor, D. (2015). History of the development of the East African Rift System: A series of interpreted maps through time. *Journal of African Earth Sciences*, *101*, 232–252. https://doi.org/10.1016/j.jafrearsci.2014.09.016

McCall, G. J. H. (1967). *Geology of the Nakuru-Thomson's Falls-Lake Hannington area degree sheet No. 35, S.W. quarter, and 43, N.W. quarter*. Survey, Ministry, Republic of Kenya.

Morley, C. K. (2010). Stress re-orientation along zones of weak fabrics in rifts: An explanation for pure extension in 'oblique' rift segments? *Earth and Planetary Science Letters*, *297*(3–4), 667–673. https://doi.org/10.1016/j.epsl.2010.07.022

Morley, C. K., Wescott, W. A., Stone, D. M., Harper, R. M., Wigger, S. T., & Karanja, F. M. (1992). Tectonic evolution of the northern Kenyan Rift. *Journal of the Geological Society*, *149*(3), 333–348. https://doi.org/10.1144/gsjgs.149.3.0333

Moucha, R., & Forte, A. M. (2011). Changes in African topography driven by mantle convection. *Nature Geoscience*, *4*(10), 707–712. https://doi.org/10.1038/ngeo1235

Mugisha, F., Ebinger, C. J., Strecker, M., & Pope, D. (1997). Two-stage rifting in the Kenya rift: Implications for half-graben models. *Tectonophysics*, *278*(1–4), 63–81. https://doi.org/10.1016/S0040-1951(97)00095-4

Muirhead, J. D., & Kattenhorn, S. A. (2018). Activation of preexisting transverse structures in an evolving magmatic rift in East Africa. *Journal of Structural Geology*, *106*, 1–18. https://doi.org/10.1016/j.jsg.2017.11.004

Muirhead, J. D., Kattenhorn, S. A., & Le Corvec, N. (2015). Varying styles of magmatic strain accommodation across the East African Rift. *Geochemistry, Geophysics, Geosystems*, *16*(8), 2775–2795. https://doi.org/10.1002/2015GC005918

Muirhead, J. D., Kattenhorn, S. A., Lee, H., Mana, S., Turrin, B. D., Fischer, T. P., et al. (2016). Evolution of upper crustal faulting assisted by magmatic volatile release during early-stage continental rift development in the East African Rift. *Geosphere*, *12*(6), 1670–1700. https://doi.org/10.1130/GES01375.1

Mulibo, G. D., & Nyblade, A. A. (2013). The P and S wave velocity structure of the mantle beneath eastern Africa and the African superplume anomaly. *Geochemistry, Geophysics, Geosystems*, *14*(8), 2696–2715. https://doi.org/10.1002/ggge.20150

Muluneh, A. A., Brune, S., Illsley-Kemp, F., Corti, G., Keir, D., Glerum, A., et al. (2020). Mechanism for deep crustal seismicity: Insight from modeling of deformation process at the Main Ethiopian Rift. *Geochemistry, Geophysics, Geosystems*, *21*(7), e2020GC008935. https://doi.org/10.1029/2020GC008935

Naliboff, J. B., Buiter, S. J. H., Péron-Pinvidic, G., Osmundsen, P. T., & Tetreault, J. (2017). Complex fault interaction controls continental rifting. *Nature Communications*, *8*(1), 1179. https://doi.org/10.1038/s41467-017-00904-x

Naliboff, J. B., Glerum, A., Brune, S., Péron-Pinvidic, G., & Wrona, T. (2020). Development of 3D rift heterogeneity through fault network evolution. *Geophysical Research Letters*, e2019GL086611. *47*(13), https://doi.org/10.1029/2019GL086611

Neuharth, D., Brune, S., Glerum, A., Heine, C., & Welford, J. K. (2021). Formation of continental microplates through rift linkage: Numerical modeling and its application to the Flemish Cap and Sao Paulo Plateau. *Geochemistry, Geophysics, Geosystems*, e2020GC009615. *22*(4), https://doi.org/10.1029/2020GC009615

Oliva, S. J., Ebinger, C. J., Wauthier, C., Muirhead, J. D., Roecker, S. W., Rivalta, E., & Heimann, S. (2019). Insights into fault-magma interactions in an early-stage continental rift from source mechanisms and correlated volcano-tectonic earthquakes. *Geophysical Research Letters*, *46*(4), 2065–2074. https://doi.org/10.1029/2018GL080866

Osei Tutu, A., Steinberger, B., Sobolev, S. V., Rogozhina, I., & Popov, A. A. (2018). Effects of upper mantle heterogeneities on the lithospheric stress field and dynamic topography. *Solid Earth*, *9*(3), 649–668. https://doi.org/10.5194/se-9-649-2018

Peron-Pinvidic, G., Manatschal, G., & the "IMAGinING RIFTING" Workshop Participants (2019). Rifted margins: State of the art and future challenges. *Frontiers of Earth Science*, *7*. https://doi.org/10.3389/feart.2019.00218

Persaud, P., Tan, E., Contreras, J., & Lavier, L. (2017). A bottom-driven mechanism for distributed faulting in the Gulf of California rift. *Tectonophysics*, *719–720*, 51–65. https://doi.org/10.1016/j.tecto.2016.11.024

Petersen, K. D., & Schiffer, C. (2016). Wilson cycle passive margins: Control of orogenic inheritance on continental breakup. *Gondwana Research*, *39*, 131–144. https://doi.org/10.1016/j.gr.2016.06.012

Petit, C., & Deverchere, J. (2006). Structure and evolution of the Baikal rift: A synthesis. *Geochemistry, Geophysics, Geosystems*, *7*(11). https://doi.org/10.1029/2006GC001265

Pérez-Gussinyé, M., Andrés-Martínez, M., Araújo, M., Xin, Y., Armitage, J., & Morgan, J. P. (2020). Lithospheric strength and rift migration controls on synrift stratigraphy and breakup unconformities at rifted margins: Examples from numerical models, the Atlantic and South China Sea mar-gins. *Tectonics*, *39*, e2020TC006255.

Phillips, T. B., Jackson, C. A.-L., Bell, R. E., Duffy, O. B., & Fossen, H. (2016). Reactivation of intrabasement structures during rifting: A case study from offshore southern Norway. *Journal of Structural Geology*, *91*, 54–73. https://doi.org/10.1016/j.jsg.2016.08.008

Pik, R., Marty, B., & Hilton, D. R. (2006). How many mantle plumes in Africa? The geochemical point of view. *Chemical Geology*, *226*(3–4), 100–114. https://doi.org/10.1016/j.chemgeo.2005.09.016

Plasman, M., Tiberi, C., Ebinger, C., Gautier, S., Albaric, J., Peyrat, S., et al. (2017). Lithospheric low-velocity zones associated with a magmatic segment of the Tanzanian Rift, East Africa. *Geophysical Journal International*, *210*(1), 465–481. https://doi.org/10.1093/gji/ggx177

Randel, R. P., & Johnson, R. W. (1970). *Geological map of the Suswa area*. Kenya: Ministry of Natural Resources, Mines & Geological Department.

Riedl, S., Melnick, D., Mibei, G. K., Njue, L., & Strecker, M. R. (2020). Continental rifting at magmatic centers: Structural implications from the Late Quaternary Menengai Caldera, central Kenya Rift. *Journal of the Geological Society*, *177*(1), 153–169. https://doi.org/10.1144/jgs2019-021

Ring, U. (2014). The East African Rift system. *Austrian Journal of Earth Sciences*, *107*(1).

Robertson, E. A. M., Biggs, J., Cashman, K. V., Floyd, M. A., & Vye-Brown, C. (2015). Influence of regional tectonics and pre-existing structures on the formation of elliptical calderas in the Kenyan Rift. *Geological Society, London, Special Publications*, *420*(1), 43–67. https://doi.org/10.1144/SP420.12

Rooney, T. O. (2020). The Cenozoic magmatism of East Africa: Part II – Rifting of the mobile belt. *Lithos*, *360–361*, 105291. https://doi.org/10.1016/j.lithos.2019.105291

Rooney, T. O., Herzberg, C., & Bastow, I. D. (2012). Elevated mantle temperature beneath East Africa. *Geology*, *40*(1), 27–30. https://doi.org/10.1130/G32382.1

Ros, E., Pérez-Gussinyé, M., Araújo, M., Thoaldo Romeiro, M., Andrés-Martínez, M., & Morgan, J. P. (2017). Lower crustal strength controls on melting and serpentinization at magma-poor margins: Potential implications for the South Atlantic. *Geochemistry, Geophysics, Geosystems, 18*(12), 4538–4557. https://doi.org/10.1002/2017GC007212

Rose, I., Buffett, B., & Heister, T. (2017). Stability and accuracy of free surface time integration in viscous flows. *Physics of the Earth and Planetary Interiors*, *262*, 90–100. https://doi.org/10.1016/j.pepi.2016.11.007

Rowland, J. V., Baker, E., Ebinger, C. J., Keir, D., Kidane, T., Biggs, J., et al. (2007). Fault growth at a nascent slow-spreading ridge: 2005 Dabbahu rifting episode, Afar. *Geophysical Journal International*, *171*(3), 1226–1246. https://doi.org/10.1111/j.1365-246X.2007.03584.x

Rutter, E. H., & Brodie, K. H. (2004). Experimental grain size-sensitive flow of hot-pressed Brazilian quartz aggregates. *Journal of Structural Geology*, *26*(11), 2011–2023. https://doi.org/10.1016/j.jsg.2004.04.006

Rybacki, E., Gottschalk, M., Wirth, R., & Dresen, G. (2006). Influence of water fugacity and activation volume on the flow properties of fine-grained anorthite aggregates. *Journal of Geophysical Research*, *111*(B3). https://doi.org/10.1029/2005JB003663

Saggerson, E. P. (1970). The structural control and genesis of alkaline rocks in central Kenya. *Bulletin of Volcanology*, *34*(1), 38–76. https://doi.org/10.1007/BF02597779

Saggerson, E. P. (1991). *Geology of the Nairobi area, degree sheet 51, NE Quarter*. Geological Survey of Kenya Report No. 98, Nairobi, Kenya: Ministry of Environment and Natural Resources, Mines and Geological Department.

Salazar-Mora, C. A., Huismans, R. S., Fossen, H., & Egydio-Silva, M. (2018). The Wilson cycle and effects of tectonic structural inheritance on rifted passive margin formation. *Tectonics*, *37*(9), 3085–3101. https://doi.org/10.1029/2018TC004962

Sandiford, D., Brune, S., Glerum, A., Naliboff, J., & Whittaker, J. M. (2021). Kinematics of footwall exhumation at oceanic detachment faults: Solid-block rotation and apparent unbending. *Geochemistry, Geophysics, Geosystems*, e2021GC009681. *22*(4), https://doi.org/10.1029/2021GC009681

Saria, E., Calais, E., Stamps, D. S., Delvaux, D., & Hartnady, C. J. H. (2014). Present-day kinematics of the East African Rift. *Journal of Geophysical Research: Solid Earth*, *119*(4), 3584–3600. https://doi.org/10.1002/2013JB010901

Schilling, J.-G. (1991). Fluxes and excess temperatures of mantle plumes inferred from their interaction with migrating mid-ocean ridges. *Nature*, *352*(6334), 397–403. https://doi.org/10.1038/352397a0

Schlische, R. W.,Withjack, M. O., & Olsen, P. E. (2003). Relative timing of CAMP, rifting, continental breakup, and basin inversion: Tectonic significance. Geophysical Monograph, *136*, 33–59.

Schumacher, M. E. (2002). Upper Rhine Graben: role of preexisting structures during rift evolution. *Tectonics*, *21*(1). https://doi.org/10.1029/2001TC900022

Schwarz, M., & Henk, A. (2005). Evolution and structure of the Upper Rhine Graben: Insights from three-dimensional thermomechanical modeling. *International Journal of Earth Sciences*, *94*(4), 732–750. https://doi.org/10.1007/s00531-004-0451-2

Shackleton, R. M. (1945). *Geology of the Nyeri area*. Geological Survey of Kenya Report No. 12.

Shackleton, R. M. (1976). A Discussion on global tectonics in Proterozoic times-Pan-African Structures. *Philosophical Transactions of the Royal Society of London - Series A: Mathematical and Physical Sciences*, *280*(1298), 491–497. https://doi.org/10.1098/rsta.1976.0008

Shackleton, R. M. (1978). Structural development of the East African Rift system. *Geological Society, London, Special Publications*, *6*(1), 19–28. https://doi.org/10.1144/GSL.SP.1978.006.01.04

Shackleton, R. M. (1993). Tectonics of the Mozambique Belt in East Africa. *Geological Society, London, Special Publications*, *76*(1), 345–362. http://dx.doi.org/10.1144/GSL.SP.1993.076.01.17

Shackleton, R. M., & Ries, A. C. (1984). The relation between regionally consistent stretching lineations and plate motions. *Journal of Structural Geology*, *6*(1–2), 111–117. https://doi.org/10.1016/0191-8141(84)90089-0

Sharples, W., Moresi, L.-N., Jadamec, M. A., & Revote, J. (2015). Styles of rifting and fault spacing in numerical models of crustal extension. *Journal of Geophysical Research: Solid Earth*, *120*(6), 4379–4404. https://doi.org/10.1002/2014JB011813

Sippel, J., Meeßen, C., Cacace, M., Mechie, J., Fishwick, S., Heine, C., et al. (2017). The Kenya rift revisited: Insights into lithospheric strength through data-driven 3-D gravity and thermal modeling. *Solid Earth*, *8*(1), 45–81. https://doi.org/10.5194/se-8-45-2017

Smith, M. (1994). Stratigraphic and structural constraints on mechanisms of active rifting in the Gregory Rift, Kenya. *Tectonophysics*, *236*(1–4), 3–22. https://doi.org/10.1016/0040-1951(94)90166-X

Smith, M., & Mosley, P. (1993). Crustal heterogeneity and basement influence on the development of the Kenya Rift, East Africa. *Tectonics*, *12*(2), 591–606. https://doi.org/10.1029/92TC01710

Sobolev, S. V., Sobolev, A. V., Kuzmin, D. V., Krivolutskaya, N. A., Petrunin, A. G., Arndt, N. T., et al. (2011). Linking mantle plumes, large igneous provinces and environmental catastrophes. *Nature*, *477*(7364), 312–316. https://doi.org/10.1038/nature10385

Sokoutis, D., Corti, G., Bonini, M., Pierre Brun, J., Cloetingh, S., Mauduit, T., & Manetti, P. (2007). Modeling the extension of heterogeneous hot lithosphere. *Tectonophysics*, *444*(1–4), 63–79. https://doi.org/10.1016/j.tecto.2007.08.012

Stab, M., Bellahsen, N., Pik, R., Quidelleur, X., Ayalew, D., & Leroy, S. (2015). Modes of rifting in magma-rich settings: Tectono-magmatic evolution of Central Afar. *Tectonics*, *35*(1), 2–38. https://doi.org/10.1002/2015TC003893

Stamps, D. S., Calais, E., Saria, E., Hartnady, C., Nocquet, J. M., Ebinger, C. J., & Fernandes, R. M. (2008). A kinematic model for the East African Rift. *Geophysical Research Letters*, *35*(5). https://doi.org/10.1029/2007GL032781

Stamps, D. S., Iaffaldano, G., & Calais, E. (2015). Role of mantle flow in Nubia-Somalia plate divergence. *Geophysical Research Letters*, *42*(2), 290–296. https://doi.org/10.1002/2014GL062515

Strecker, M. R. (1991). *Das zentrale und südliche Kenia-Rift unter besonderer Berücksichtigung der neotektonischen Entwicklung* (Habilitation thesis). University of Karlsruhe.

Strecker, M. R., Blisniuk, P. M., & Eisbacher, G. H. (1990). Rotation of extension direction in the central Kenya Rift. *Geology*, *18*(4), 299. https://doi.org/10.1130/0091-7613(1990)018<0299:ROEDIT>2.3.CO;2

Supak, S., Bohnenstiehl, D., & Buck, W. (2006). Flexing is not stretching: An analogue study of flexure-induced fault populations. *Earth and Planetary Science Letters*, *246*(1), 125–137. https://doi.org/10.1016/j.epsl.2006.03.028

Svartman Dias, A. E., Lavier, L. L., & Hayman, N. W. (2015). Conjugate rifted margins width and asymmetry: The interplay between lithospheric strength and thermomechanical processes. *Journal of Geophysical Research: Solid Earth*, *120*(12), 8672–8700. https://doi.org/10.1002/2015JB012074

Tetreault, J. L., & Buiter, S. J. H. (2018). The influence of extension rate and crustal rheology on the evolution of passive margins from rifting to break-up. *Tectonophysics*, *746*, 155–172. https://doi.org/10.1016/j.tecto.2017.08.029

Thompson, A. O., & Dodson, R. G. (1963). Geology of the Naivasha area. *Geological Survey of Kenya Report* No. *55*, pp. 1–80.

Thybo, H., Maguire, P. K. H., Birt, C., & Perchuć, E. (2000). Seismic reflectivity and magmatic underplating beneath the Kenya Rift. *Geophysical Research Letters*, *27*(17), 2745–2748. https://doi.org/10.1029/1999GL011294

Tiercelin, J.-J., & Lezzar, K.-E. (2002). A 300 million years history of rift lakes in Central and East Africa: An updated broad review. In *The East African great lakes: Limnology, palaeolimnology and biodiversity* (pp. 3–60). Dordrecht: Springer. https://doi.org/10.1007/0-306-48201-0_1

Tongue, J. A., Maguire, P. K. H., & Young, P. A. V. (1992). Seismicity distribution from temporary earthquake recording networks in Kenya. *Tectonophysics*, *204*(1–2), 71–79. https://doi.org/10.1016/0040-1951(92)90270-G

Torres Acosta, V., Bande, A., Sobel, E. R., Parra, M., Schildgen, T. F., Stuart, F., & Strecker, M. R. (2015). Cenozoic extension in the Kenya Rift from low-temperature thermochronology: Links to diachronous spatiotemporal evolution of rifting in East Africa. *Tectonics*, *34*(12), 2367–2386. https://doi.org/10.1002/2015TC003949

Tugume, F., Nyblade, A., & Julià, J. (2012). Moho depths and Poisson's ratios of Precambrian crust in East Africa: Evidence for similarities in Archean and Proterozoic crustal structure. *Earth and Planetary Science Letters*, *355–356*(356), 73–81. https://doi.org/10.1016/j.epsl.2012.08.041

Ulvrova, M. M., Brune, S., & Williams, S. (2019). Breakup Without Borders: How Continents Speed Up and Slow Down During Rifting. *Geophysical Research Letters*, *46*(3), 1338–1347. https://doi.org/10.1029/2018GL080387

Weinstein, A., Oliva, S. J., Ebinger, C. J., Roecker, S., Tiberi, C., Aman, M., et al. (2017). Fault-magma interactions during early continental rifting: Seismicity of the Magadi-Natron-Manyara basins, Africa. *Geochemistry, Geophysics, Geosystems*, *18*(10), 3662–3686. https://doi.org/10.1002/2017GC007027

Wichura, H., Bousquet, R., Oberhänsli, R., Strecker, M. R., & Trauth, M. H. (2010). Evidence for middle Miocene uplift of the East African Plateau. *Geology*, *38*(6), 543–546. https://doi.org/10.1130/G31022.1

Wichura, H., Jacobs, L. L., Lin, A., Polcyn, M. J., Manthi, F. K., Winkler, D. A., et al. (2015). A 17-My-old whale constrains onset of uplift and climate change in East Africa. *Proceedings of the National Academy of Sciences of the United States of America*, *112*(13), 3910–3915. https://doi.org/10.1073/pnas.1421502112

Williams, L. A. J. (1969a). Geochemistry and petrogenesis of the Kilimanjaro volcanic rocks of the Amboseli area, Kenya. *Bulletin of Volcanology*, *33*(3), 862–888. https://doi.org/10.1007/BF02596754

Williams, L. A. J. (1969b). Volcanic associations in the Gregory rift valley, east Africa. *Nature*, *224*(5214), 61–64. https://doi.org/10.1038/224061a0

Williams, L. A. J. (1972). The Kenya rift volcanics: a note on volumes and chemical composition. *Tectonophysics*, *15*(1–2), 83–96. https://doi.org/10.1016/0040-1951(72)90054-6

Withjack, M. O., Schlische, R. W., Malinconico, M. L., & Olsen, P. E. (2013). Rift-basin development: Lessons from the Triassic-Jurassic Newark Basin of eastern North America. *Geological Society, London, Special Publications*, *369*(1), 301–321. https://doi.org/10.1144/SP369.13

Wright, T. J., Ebinger, C., Biggs, J., Ayele, A., Yirgu, G., Keir, D., & Stork, A. (2006). Magma-maintained rift segmentation at continental rupture in the 2005 Afar dyking episode. *Nature*, *442*(7100), 291–294. https://doi.org/10.1038/nature04978

Zielke, O., & Strecker, M. R. (2009). Recurrence of Large Earthquakes in Magmatic Continental Rifts: Insights from a Paleoseismic Study along the Laikipia-Marmanet Fault, Subukia Valley, Kenya Rift. *Bulletin of the Seismological Society of America*, *99*(1), 61–70. https://doi.org/10.1785/0120080015

Zwaan, F., Schreurs, G., & Rosenau, M. (2019). Rift propagation in rotational versus orthogonal extension: Insights from 4D analogue models. *Journal of Structural Geology*, *135*, 103946. https://doi.org/10.1016/j.jsg.2019.103946